Title

Triclosan targets miR-144 abnormal expression to induce neurodevelopmental toxicity mediated by activating PKC/MAPK signaling pathway

Authors

Diao, Wenqi
Qian, Qiuhui
Sheng, Guangyao
et al.

Publication Date

2022-06-01

DOI

10.1016/j.jhazmat.2022.128560

Peer reviewed

Journal of Hazardous Materials 431 (2022) 128560

Contents lists available at ScienceDirect

Journal of Hazardous Materials

journal homepage: www.elsevier.com/locate/jhazmat

Research Paper

Triclosan targets miR-144 abnormal expression to induce neurodevelopmental toxicity mediated by activating PKC/MAPK signaling pathway

Wenqi Diao [a,b,1], Qiuhui Qian [a,1], Guangyao Sheng [a], Anfei He [a], Jin Yan [a], Randy A. Dahlgren [c], Xuedong Wang [a,*,2], Huili Wang [b,a,**,2]

[a] School of Environmental Science and Engineering, Suzhou University of Science and Technology, Suzhou 215009, PR China
[b] School of Laboratory Medicine and Life Sciences, Wenzhou Medical University, Wenzhou 325035, PR China
[c] Department of Land, Air and Water Resources, University of California, Davis, CA 95616, USA

HIGHLIGHTS

- Dre-miR-144 was screened and up-regulated under TCS exposure from zebrafish by RNA-seq.
- Up-regulation of miR-144 caused neurodevelopment toxicity and abnormal motor behavior.
- MiR-144 up-regulation induced neurotoxicity by repressing neurodevelopment related genes *cd*36, *syn*2a, and *epas*1b.
- Activation of nuclear transcription factor on PKC/MAPK can bind and promoted mir-144 transcription activity.
- TCS acted on GPER to activate downstream pathway PKC/MAPK and result in miR-144 up-regulation.

GRAPHICAL ABSTRACT

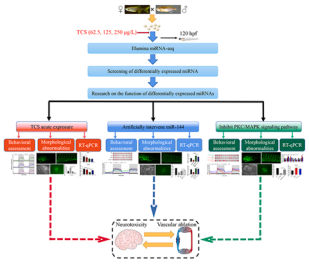

ARTICLE INFO

Editor: <Nan Sang>

Keywords:
Triclosan
Zebrafish
MiR-144
Neurodevelopmental toxicity
PKC/MAPK signaling pathway

ABSTRACT

Although the previous research confirmed that triclosan (TCS) induced an estrogen effect by acting on a novel G-protein coupled estrogen-membrane receptor (GPER), the underlying mechanisms by which downstream pathways induce neurotoxicity remain unclear after TCS activation of GPER. By employing a series of techniques (Illumina miRNA-seq, RT-qPCR, and artificial intervention of miRNA expression), we screened out four important miRNAs, whose target genes were directly/indirectly involved in neurodevelopment and neurobehavior. Especially, the miR-144 up-regulation caused vascular malformation and severely affected hair-cell development and lateral-line-neuromast formation, thereby causing abnormal motor behavior. After microinjecting 1–2-cell embryos, the similar phenotypic malformations as those induced by TCS were observed, including aberrant neuromast, cuticular-plate development and motor behavior. By KEGG pathway enrichment analysis, these target genes were demonstrated to be mainly related to the PKC/MAPK signaling pathway. When a PKC inhibitor

* Corresponding author.
** Corresponding author at: School of Environmental Science and Engineering, Suzhou University of Science and Technology, Suzhou 215009, PR China.
E-mail addresses: zjuwxd@163.com (X. Wang), whuili@163.com (H. Wang).
[1] Co-first author: Wenqi Diao and Qiuhui Qian are the co-first autho
[2] 8247000

https://doi.org/10.1016/j.jhazmat.2022.128560
Received 17 December 2021; Received in revised form 16 February 2022; Accepted 22 February 2022
Available online 24 February 2022

was used to suppress the PKC/MAPK pathway, a substantial alleviation of TCS-induced neurotoxicity was observed. Therefore, TCS acts on GPER to activate the downstream PKC/MAPK signaling pathway, further up-regulating miR-144 expression and causing abnormal modulation of these nerve-related genes to trigger neurodevelopmental toxicity. These findings unravel the molecular mechanisms of TCS-induced neurodegenerative diseases, and offer theoretical guidance for TCS-pollution early warning and management.

1. Introduction

As a broad-spectrum antibacterial agent, triclosan (TCS, 5-chloro-2-(2,4-dichlorophenoxy)phenol) is widely used in household chemicals and disinfectants for medical devices and textiles (Bedoux et al., 2012). Due to its widespread use, TCS and its derivatives are universally detected in rivers (0.0002–9.65 μg/L), sediments (5.11–50.36 μg/kg), influent and effluent of wastewater treatment plants (0.148–86.2 μg/L; 0–5.037 μg/L), biosolids (2.16–13.5 μg/kg), raw sludge (3.65–15.0 μg/kg) and fish (1040 μg/kg) (Jagini et al., 2019; Kumar et al., 2018). Most notably, TCS has the potential for bioaccumulation and long-term retention in the environment and organisms owing to its lipophilicity and persistence (Dhillon et al., 2015). TCS was widely detected in amniotic fluid, maternal urine, cord serum and maternal serum samples with detection rates up to 76.9% (Wang et al., 2013). As such, there is growing concern for its potential negative impacts on human health. As a common endocrine-disrupting chemical (EDC), TCS has garnered considerable attention owing to the correlation between TCS chronic exposure during gestation and abnormal behavior in children. Previous studies demonstrated that TCS can accumulate in the brain and cause histopathological or functional damage to the nervous system (Orvos et al., 2002). TCS was also shown to impair hippocampal neuronal function and spatial memory in male rats (Ishibashi et al., 2004). Further, TCS may inhibit neural stem cell viability and survival, inducing neurodegenerative effects in developing rat brains (Yueh and Tukey, 2016). Moreover, the swimming behavior of *Pimephales promelas* was prominently affected even after short-term (1-day) exposure to 75 μg/L TCS (Schultz et al., 2012). TCS was also demonstrated to cause neurotoxicity arising from DNA fragmentation and apoptosis in primary cultures of neocortical neurons (Szychowski et al., 2015). Finally, TCS can interfere with the proper functioning of Ca^{2+} signaling channels, thus delaying trunk muscle development in zebrafish (Delov et al., 2014).

In recent years, TCS was documented to have an estrogenic effect through targeting a new type of G-protein coupled estrogen membrane receptor (GPER) (Wang et al., 2021). Previous research by our group documented that TCS exposure activated GPER to trigger an estrogen effect (Huang et al., 2020). GPER is a non-classical estrogen receptor binding to the plasma membrane through seven transmembrane domains, it is widely distributed in the brain functional area related to emotion control, serving an important role in regulation of the HPA axis and mood (Zheng et al., 2020). Recently, several additional EDCs were reported to activate GPER-related pathways, with subsequent triggering of underlying neurotoxic and estrogenic effects. Both TmCP and TpCP were confirmed to have negative effects on nerve-electrical activity and neurite outgrowth, which offer strong evidence regarding the association of TCP neurotoxicity with their roles in GPER (Rettberg et al., 2014). However, after TCS activation of GPER, the underlying mechanisms by which downstream pathways induce neurotoxicity remain unclear.

MicroRNAs (miRNAs), as epigenetic biomarkers, are a class of short non-coding RNAs that regulate the translation and stability of targeting mRNAs (Bianchi et al., 2012). Each miRNA is partially or perfectly complementary to the 3′-UTR regions of one or more mRNA transcripts, fulfilling functions as negative regulators of gene expression (Wang et al., 2011), and regulating some pathways or gene post-transcriptional networks. These molecules play key roles in the regulation of cellular responses. For example, miR-144 displays significant changes in blood diseases, cancer, nervous system and heart diseases (Tian et al., 2021; Katsuura et al., 2012; Liu et al., 2012). Currently, most miR-144 research focuses on the blood system, but few studies addressing the higher morbidity associated with psychiatric diseases. The miR-144 is involved in the growth of neurites, neurogenesis and signal transmission of PTEN, ERK and Wnt/β-catenin pathways (Zhou et al., 2009). Li and coworkers (Li et al., 2018) reported that the inhibition of miR-144-3P reduced neuronal damage caused by hypoxia or reoxygenation. Because miRNAs exert biological functions by regulating downstream target genes, knowledge of their upstream mechanisms is required to predict and trace the abnormal expression of miR-144. To date, information concerning miR-144 is extremely scarce in zebrafish development research. Therefore, it is highly warranted to explore the regulatory mechanism of miR-144 on neural development upon TCS exposure in zebrafish.

Zebrafish (*Danio rerio*) are an experimental animal model and highly homologous making them an excellent organism in which to evaluate developmental neurotoxicity (Cansız et al., 2021). Although miR-144 was predicted to be highly enriched in the brain (Zhou et al., 2019), the mechanism by which TCS induces estrogen effects has not been addressed from the perspective of miR-144 regulation. Based on our previous research, GPER was activated in zebrafish following TCS exposure (Huang et al., 2020; Wang et al., 2020) Bioinformatics analysis and a series of experiments verified that the abnormal expression of miR-144 could cause neurotoxicity to zebrafish larvae, and the underlying upstream pathways triggering miR-144 abnormal expression were further examined after GPER was activated by TCS. Collectively, the results of previous studies inferred that the PKC/MAPK signaling pathway was involved in the process of TCS-induced neurotoxicity. These findings are conducive to understanding the molecular mechanisms of TCS-induced neurotoxicity and neurodegenerative diseases, and also offer important guidance for TCS-pollution early warning and management.

2. Materials and methods

2.1. Chemical reagents and zebrafish maintenance

TCS with a purity of 99.9% was purchased from Sigma-Aldrich (St. Louis, USA). Chromatographic-grade acetone was acquired from China Pesticide Chemical Corporation (Shenyang, China). TRIzol RNA extraction and reverse transcription kits were purchased from Takara (Dalian, China). DASPEI and Mitoxantrone hydrochloride (MTO) were obtained from J&K Scientific (Beijing, China).

Zebrafish used in this investigation included wild-type AB strain and transgene line Tg (*fli-1*: EGFP), which were gratis supplied by the Aquatic Biology Laboratory, Chinese Academy of Sciences (Wuhan, China). Zebrafish maintenance was carried out based on our group's previous report (Li et al., 2016).

2.2. TCS acute exposure

TCS concentrations were selected on the basis of their environmentally related concentrations, LC_{50} and EC_{50} indicators, and our previous experimental trials (Ling et al., 2020). Four TCS-exposure treatments were set: 0 (control), 62.5, 125 and 250 μg/L, among which 0.0025% acetone was added to the control group to examine the solvent effect on zebrafish growth and development. As for acute exposure, each well in a 96-well plate contained 200 μL of solution and one embryo, which was

raised and observed in the 6–120-hpf time-window.

2.3. Bioinformatics analysis, synthesis and microinjection of miR-144 mimics and inhibitors

The 5-dpf zebrafish were independently exposed to four TCS concentrations (0, 62.5, 125, 250 μg/L) for miRNA sequencing. According to manufacturer's instructions (LC Sciences, Houston, USA), we strictly carried out the corresponding quality control along with the sequencing of all libraries.

The mimics and inhibitors of miR-144–3p were synthesized by Shanghai GenePharma (Shanghai, China), and the synthesized sequences were 5′-UACAGUAUAGAUGAUGUACU-3′ for mimic and AGUACAUCAUCUAUACUGUA for inhibitor. The synthesized sequences for the negative control were 5′-UUCUCCGAACGUGUCACGUTT-3′ for sense and 5′-ACGUGACACGUUCGGAGAATT-3′ for antisense. With regard to microinjection, miR-144 mimics and inhibitors were firstly diluted according to the instructions, and then injected into 1–2-cell stage.

2.4. Observation of lateral hair cell staining and hair cell bundle formation

To observe the effects of TCS exposure on the expression of miR-144, the active fluorescent dye, 2-[4-(dimethylamino)styryl-N-ethylpyridinium iodine (DASPEI; Invitrogen, CAS NO: 3785–01–1, USA), was used to stain zebrafish hair cells. When the embryos in the treatment/control group developed to the 12-hpf stage, 0.5% PTU was added to the EM medium to inhibit the melanin production of the embryos. At 120-hpf, we transferred 120-hpf zebrafish juveniles into a 1.5#8201;mL centrifuge tube, and rinsed the embryos in 1 mL of PBS at 70 rpm for 5 min. After the remaining liquid was extracted, 200 μL of 0.005% DASPEI dye solution was added to each tube, and the embryos were stained for 20 min in the dark. After washing three times using 1 mL of PBS buffer, the embryos were anesthetized via 1 ×MS222 (Sigma) and observed under a fluorescence microscope. Meanwhile, a scanning electron microscope (SEM; Hitachi S-2400, Tokyo, Japan) was employed to observe the hair bundles of the L1 nerve mound in the posterolateral line of 5-dpf zebrafish.

2.5. Behavioral assessment

In order to evaluate larval behavior, we conducted autonomous movement, light and dark stimulation and acoustic stimulation experiments. The exercise time conditions, the number of light and dark cycles and the sound stimulation settings were performed on the basis of our group's previous methodology (Ling et al., 2020). The video was analyzed by an EthoVision XT software (Noldus IT, Wageningen, The Netherlands).

2.6. RT-qPCR

When exposed to TCS at 6–120 hpf, 50 larvae collected from each treatment were employed for total RNA analysis based on TRIzol reagent kits. Table S2 lists the primers for RT-qPCR, and the operations of RT-qPCR were carried out in three biological repetitions and three technical replicates per biological repetition.

2.7. Acetylcholinesterase (AChE) activity

To study the neurotransmitter transduction of zebrafish larvae, we used a standard AChE test kit (Nanjing Chengjian Institute of Bioengineering, Nanjing, China) to measure AChE activity.

2.8. Double luciferase assay

We constructed the zebrafish dual luciferase reporter vector from genomic DNA obtained from 5-dpf larvae using the Easy pure Genome DNA kit followed by PCR amplification reaction. The volume of the reaction system was 50 μL, and the amplified product was monitored and purified by 1% agarose gel electrophoresis. The purified fragments were ligated to the PEASY-Blunt Simple (full gold) cloning vector. After blue-white screening, the obtained monoclonal bacterial solution was sequenced. The sequence-corrected fragment vector was digested with *Sac*I and *Xho*I, and T4 was ligated with the same digested PGL0 plasmid. After biosynthesis of the target genes mut-3′UTR to obtain the mutant target gene, double enzyme digestion was performed, and the target fragment was connected to the PEASY-Blunt cloning vector and sequenced for verification. The sequence-corrected sequence fragments were carried out according to the previous steps. After double enzyme digestion, the mutant target fragment was ligated with pmirGL0 plasmid by T4, and transformed after T4 ligation. The bacteria was shaken and the plasmid was extracted to obtain WT-PGL0 and mut-PGL0. The obtained plasmids mixed with miR-144-mimic were injected into zebrafish embryos. After injection, the embryos were incubated for 48 h at 28 °C in a constant temperature incubator and then homogenized with a sterile grinding rod. The supernatant was transferred to a 96-well plate, and an aliquot (20 mL) of the extract was employed for luciferase detection based on a dual reporter system (Whitman et al., 2010). Table S3 lists primers and sequence for luciferase activity analysis.

2.9. Statistical analysis

The numbers of biological replicates, technical replicates and zebrafish used at different developmental stages are generalized in Table S4. Experimental data were expressed as mean ± standard deviation (n = 3). One-way analysis of variance and tukey multiple comparisons test were applied for determining statistical differences at the $p < 0.05$ (*), $p < 0.01$ (**) or $p < 0.001$ (***) levels using SPSS 19.0 software (IBM, USA).

3. Results

3.1. Screening and bioinformatics analysis of differentially expressed miRNAs

To screen the differentially expressed miRNAs, we used the Illumina Hiseq2000/2500 platform to perform transcriptional profile analysis on total miRNAs in 120-hpf zebrafish under TCS exposure and carried out the miRNAs expression analysis following (Ma et al., 2019). Sequencing abundance and QC analysis are summarized in detail in Table S1. Valid reads in each group were greater than 4.4 G and the sequencing quality met our requirements for the subsequent analysis. After comparing the treatments with control group, we screened out 19 differentially expressed miRNAs ($p < 0.05$ and Log2(|fold-change|)≥ 0.5), per million fragments mapped (FPKM) ≥ 100) (Fig. 1A), which were obtained from intersections between different treatment groups. With the aid of biological information analysis, the expression pattern changes of the 19 miRNAs were clustered using an online software tool (https://www.omicstudio.cn/tool) (Fig. 1B), and classified as three expression change types. Among them, miR-181a-5p, miR-129–3p and miR-137–5p were down-expressed with increasing TCS concentrations; by way of contrast, miR-153b-3p, miR-301a and miR-454a were down-expressed at low concentration and over-expressed at higher concentration. Other miRNAs were all over-expressed with the increasing TCS concentrations (Fig. 1B). With reference to previous reports and predictions of their regulatory target genes, we screened out miR-125b-1-3p, miR-137–5P, miR-144-3P, miR-124–5p, which were all related to the development and injury/pathology of the nervous system (Silber et al., 2008). Detailed information for the four miRNAs and their regulatory target

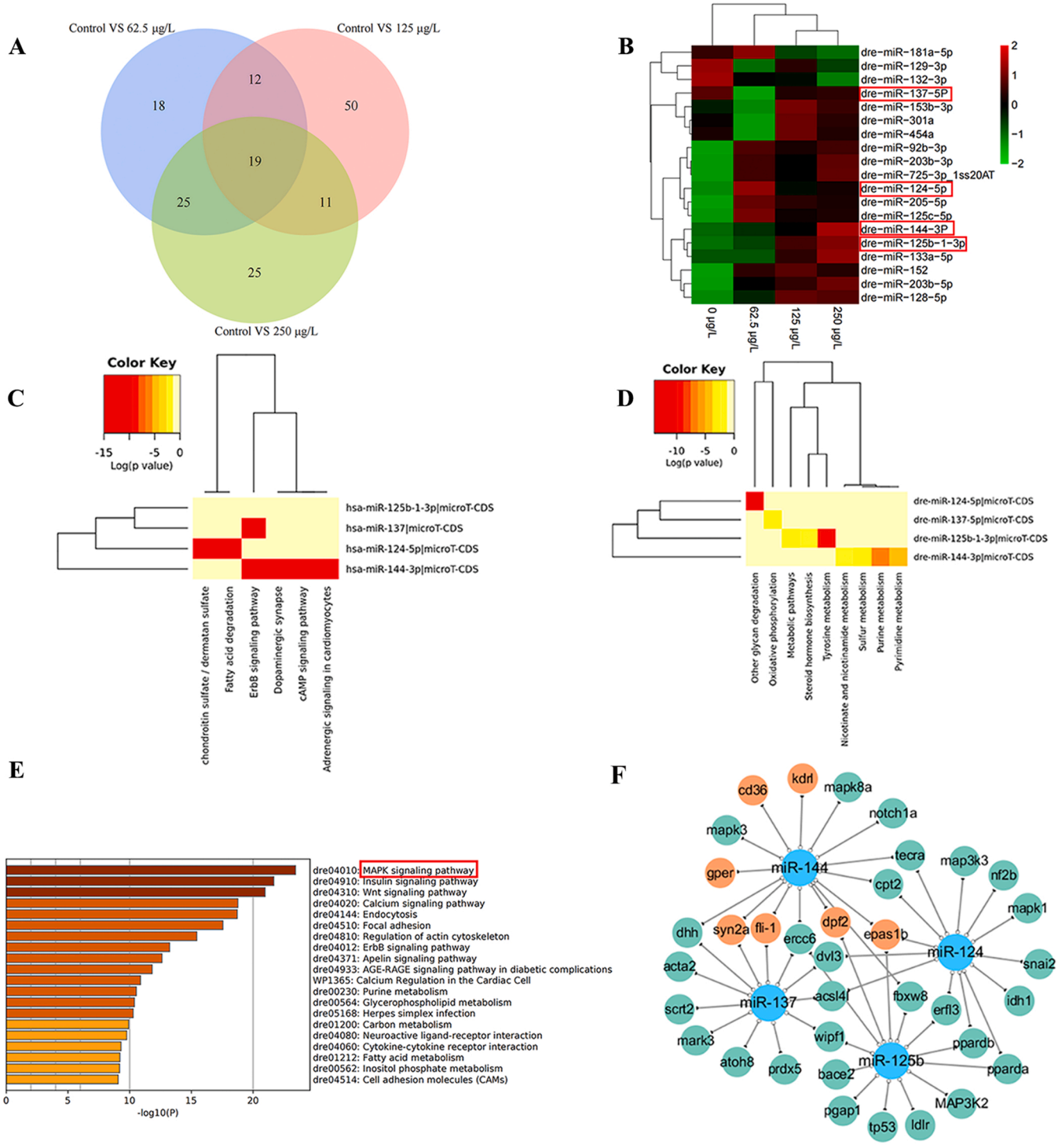

Fig. 1. Screening and bioinformatics analysis of differentially expressed miRNAs under TCS exposure. Notes: (1) A, Venn diagram for the differentially expressed miRNAs btween the treatment gtoups; (2) B, Heat map of expression change pattern of 19 terms common differentially expressed miRNAs; (3) C, Heat map and clustering patterns of four candidate diffffferentially expressed miRNAs from human (p-value threshold < 0.05 and MicroT threshold<0.08); (4) D, Heat map and clustering patterns of four candidate diffffferentially expressed miRNAs from zebrafish (p-value threshold<0.05 and MicroT threshold<0.08); (5) E, KEGG pathway analysis of dre-miR-144 target genes ($p < 0.05$ and Log2(|fold-change|)≥ 0.5); (6) F, Regulatory network of target genes of four candidate miRNAs (miR-125b, miR-124, miR-137, miR-144).

genes are summarized in Table S5. Subsequently, heatmaps of the pathways regulated by four miRNAs were generated using DIANA miRPath V3 software (http://snf-515788.vm. okeanos. grnet. gr/) from human and *Danio rerio*, respectively. According to the results of these analysis (Fig. 1C-D), we found that both hsa-miR-144–3p and hsa-miR-137 were involved in the ERBβ pathway, which participates in the formation of neural stem cells (Shimozaki, 2021). Additionally, hsa-miR-144–3p regulates dopaminergic synapse, cAMP signaling pathway and adrenergic signaling. The four pathways were closely related to neural conduction and regulation, among which, ERBβ and the cAMP signaling pathways were shown to be mediated by the estrogen receptor GPER (Witkowski et al., 2021; Zhang et al., 2020).

However, dre-miR-144–3p was mainly related to purine metabolism and pyrimidine metabolism pathways in zebrafish (Fig. 1D). As such, the focus of this study was to disclose the relationship between purine/-pyrimidine metabolism and neural development/regulation, as well as specificity for species. Subsequently, the target genes regulated by miR-144 were predicted using targetscan online (http://www.targetscan.org/fish_62/) and KEGG pathway analysis of its target genes were performed in combination with the sequencing data. The results of KEGG pathway enrichment showed that the target genes regulated by dre-miR-144 were mainly enriched in the MAPK, insulin, Wnt signaling pathways, and endocytosis. Among the pathways, the MAPK signaling pathway had the highest enrichment abundance (Fig. 1E), which played an important role in the pathogenesis of neurodegenerative disorders such as Alzheimer's and Parkinson's diseases (Mufson et al., 2012). The regulatory target genes of the four miRNAs were predicted and screened with high binding scores through TargetScan. A Cytoscape software was employed to draw a regulatory network diagram, providing a basis for further neurotoxicity research. As elaborated in Fig. 1F, *cd36*, *syn2a*,

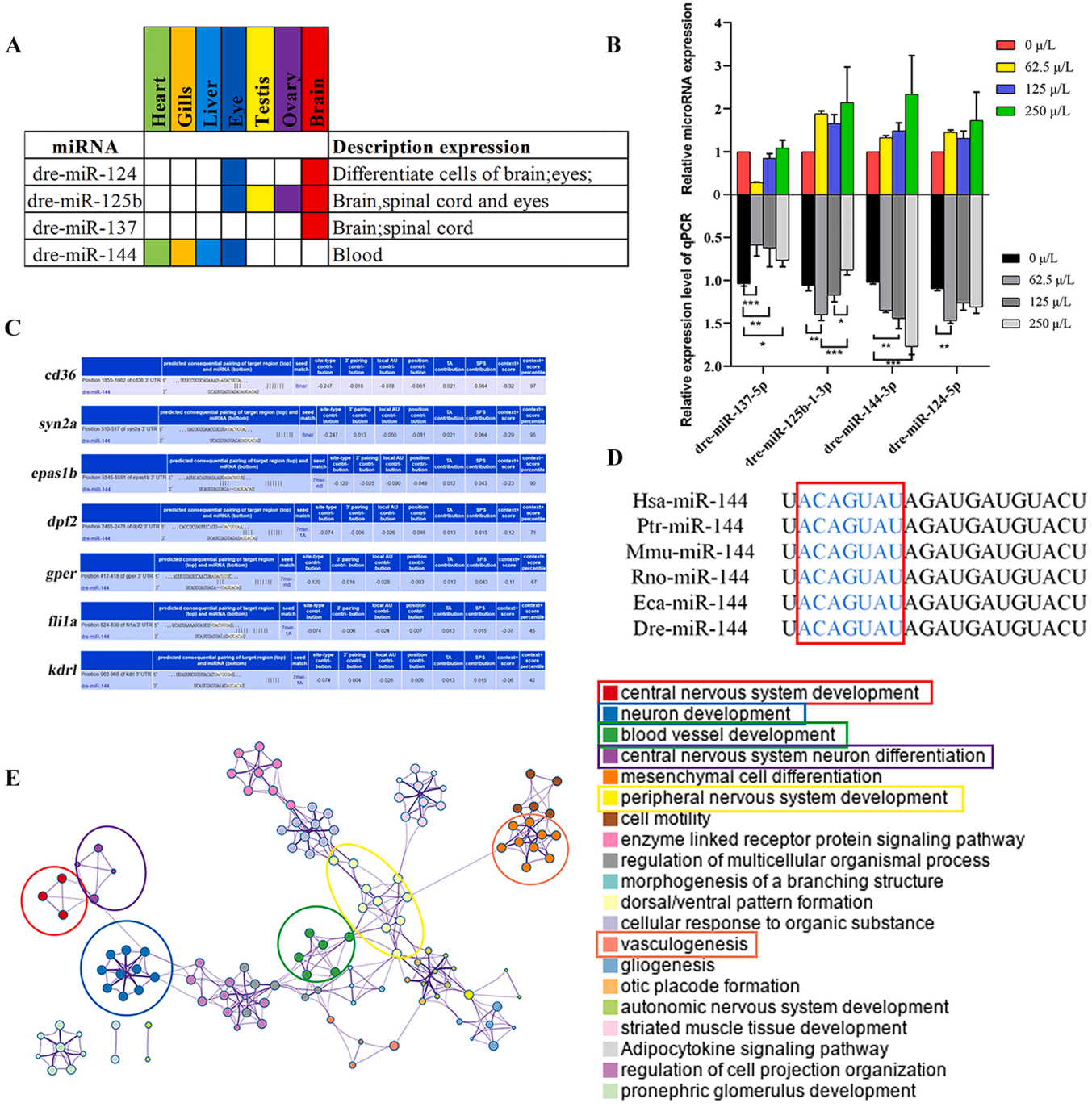

Fig. 2. The expression site and regulatory function analysis of four candidate miRNAs and the conservative of miR-144, Notes: (1) A, The expression sites of four candidate miRNAs in zebrafish; (2) B, The differential expression of miRNAs by miRNA-seq or RT-qPCR, "* ", "* *" and "* ** " indicate significance levels at $p < 0.05$, $p < 0.01$ and $p < 0.001$, respectively; (3) C, Use the targetscan website to predict the binding of target genes to miR-144; (4) D, Conservative comparison of miR-144 among different species; (5) E, Using gene function annotation analysis tool metascape to analyze the GO function enrichment of miR-144 target genes ($p < 0.05$), Color frames represent pathways related to neuro-development or vascular development.; (6) All values were expressed as mean ± standard deviation (SD) in triplicate (n = 3).

epas1b, *dpf2*, *fli1a* and *kdr1* were demonstrated to be the target genes of dre-miR-144–3p or a combined regulation genes of more than two miRNAs.

3.2. Functional analysis and expression changes of miRNAs by RT-qPCR in larvae

The expression site and distribution of miRNAs in the body are closely dependent on their functions (Wienholds et al., 2005). As depicted in Fig. 2A, dre-miR-125b, dre-miR-124 and dre-miR-137 were mainly expressed in the brain and spinal cord of zebrafish central nervous system (CNS). In contrast, dre-miR-144 was distributed in the blood system, thereby resulting in most research on dre-miR-144 focusing on formation of red blood cells and the therapeutic target of leukemia (Fu et al., 2009; Whitman et al., 2010). To further confirm the RNA-seq results, RT-qPCR was performed to verify the expression changes of the four miRNAs under TCS exposure and the primers used for the four pre-miRNAs are listed in Table S2. The changing trends of their expressions were in general agreement with the results obtained by RNA-seq (Fig. 2B) ($p < 0.05$, $p < 0.01$ & $p < 0.001$). Compared to the control group, dre-miR-144 was up-regulated in all TCS-exposed treatment groups. To estimate the genes related to neural and vascular development which were most likely regulated by miR-144, the possibility of target genes were ranked according to the score and binding free energy using TargetScan online (http://www.targetscan.org/) (Fig. 2 C). Although there is a paucity of information regarding the regulatory functions of dre-miR-144 on the nervous system, it is highly conserved among species, such as human, mice, zebrafish, *Pan troglodytes*, *Macaca musculus*, *Rattus norvegicus* and *Equus caballus* (Fig. 2D). To determine detailed information for miR-144, we conducted GO biological function enrichment of the target genes regulated by miR-144 using metascape (http://metascape.org) based on the sequencing data (Zhou et al., 2019). As can be seen from Fig. 2E, the genes regulated by miR-144 were significantly enriched in the development of diencephalon and CNS, as well as neuron growth, blood vessel development, CNS neurons differentiation, angiogenesis, etc. Building upon the above analysis, we posit that the neurotoxicity induced by TCS exposure is most likely related to the up-regulation of miR-144.

3.3. TCS acute exposure induced neurotoxicity and abnormal neurobehavior

To verify whether TCS could induce neurotoxicity, we designed a series of in vivo experiments (Fig. 3 A). The larval neurobehavior and

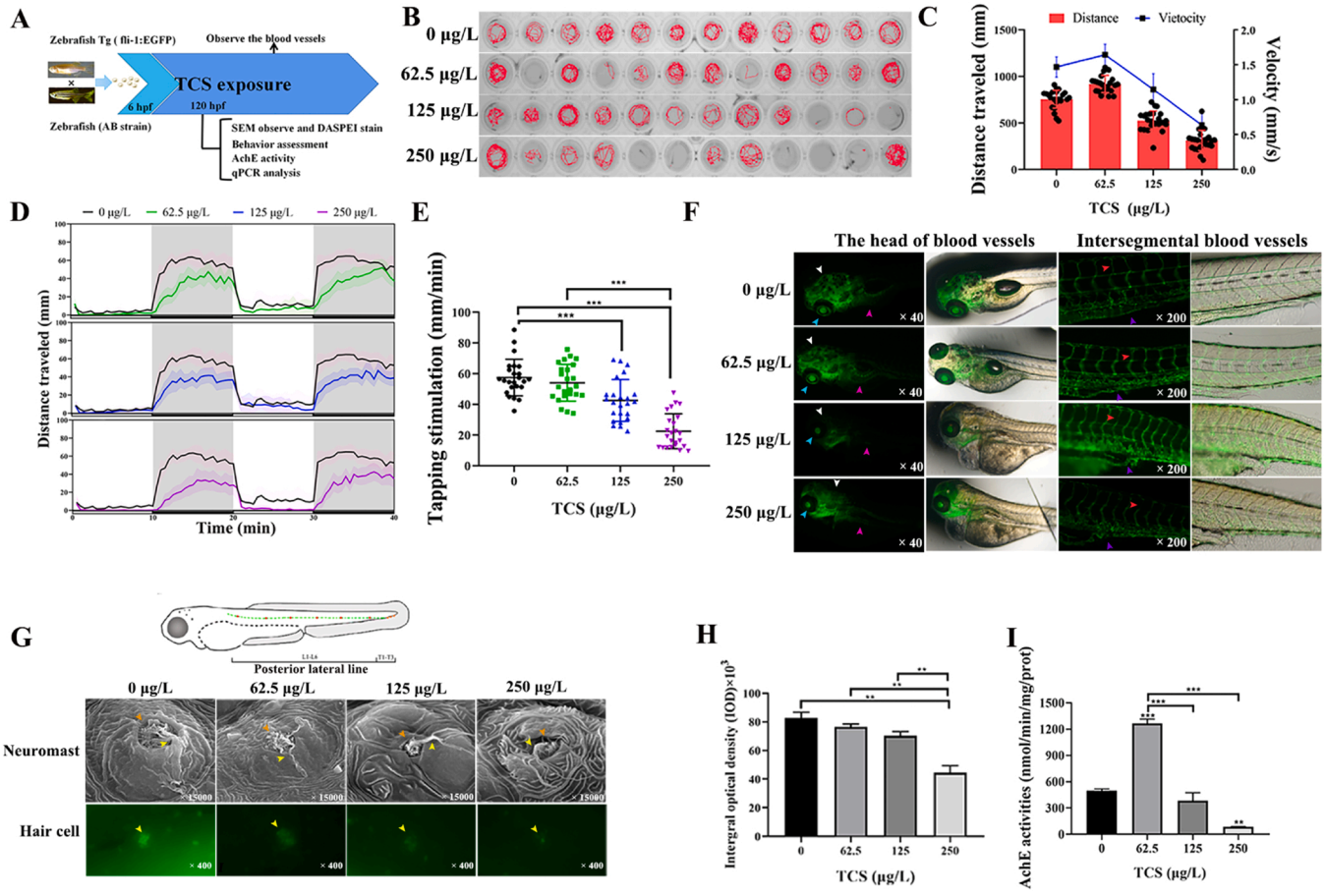

Fig. 3. TCS acute exposure induces abnormal motor behavior and influence on nerve development. Notes: (1) A, Experimental schematic diagram; (2) B, Zebrafish larvae (120 hpf) autonomous motion trajectory capture for 20 min; (3) C, Quantitative analysis of swimming distance and average speed of zebrafish larvae (120 hpf) after TCS exposure; (4) D, Effects of TCS exposure on light-dark rhythm of zebrafish larvae (120 hpf); (5) E, Effects of TCS exposure on acoustic stimulation response of zebrafish larvae (120 hpf); (6) F, Effects of TCS exposure on head (×40) and trunk (×200) blood vessel development of zebrafish larvae (120 hpf) (Left: dark field shooting; Right: bright and dark field superimposed); (7) G, Effects of TCS exposure on the neuromast development and the hair cells differentiation by scanning electron microscopy and DASPEI-staining in zebrafish larvae (120 hpf), respectively; (8) H, Quantitative analysis of hair cell number; (9) I, Effect of TCS on the activity of neurotransmitter acetylcholinesterase (AChE) in zebrafish larvae (120 hpf); (10) White arrows point to dorsal longitudinal vein (DLV), light blue arrows point to inner optic circle (IOC), purple arrows point to branchial artery, red arrows point to intersegmental vessels (ISVs), dark blue arrows point to posterior cardinal vein (PCV), orange arrows point to the L1 neuromast and yellow arrows point to L1 neuromast hair bundles; (11) All values were expressed as mean ± SD in triplicate (n = 3), "ns" means no significant difference, "* ", "* *" and "* ** " indicate significance levels at $p < 0.05$, $p < 0.01$ and $p < 0.001$, respectively.

responses to light/acoustic stimuli were recorded and quantitatively analyzed. As exhibited in Fig. 3B-C, with increasing TCS-exposure concentrations, the proportion of larval moving around gradually decreased, while those not moving at all increased. As compared to the control group (1.47 mm/s), the average swimming distance and speed were significantly higher ($p < 0.05$) in the 62.5-μg/L treatment (1.64 mm/s), whereas swim rates were lower in the 125 (1.15 mm/s) and 250-μg/L (0.64 mm/s) treatments. In the light-dark rhythm tests, zebrafish larvae showed more activity in the dark environment, while they maintained a relatively stable state when returning to the light environment, which was consistent with the motor habits of zebrafish in response to light-dark stimulation (Fig. 3D). However, compared to the control group, the swimming activities of larvae under dark conditions were significantly inhibited with increasing TCS-exposure concentrations. These findings demonstrate that TCS exposure greatly inhibited locomotor activity in the dark environment although it did not affect light-dark rhythm sensing in zebrafish larvae. As a result, we inferred that TCS slightly affected visual acuity. By means of acoustic stimulation, the larval locomotion ability was found to be significantly reduced in the 125 and 250-μg/L treatments ($p < 0.001$), but the reduction was not significant in the 62.5-μg/L treatment ($p > 0.05$) (Fig. 3E). The above findings revealed that TCS exposure severely affected the auditory response sensitivity of zebrafish or self-control of shock.

To further elucidate the underlying molecular mechanisms regarding abnormal motor behavior, a series of physiological and biochemical metrics were examined, including vascular network formation, development of lateral line neuromast and AChE activity as a neurotransmitter biomarker. The development of blood vessels in larval head and trunk were observed by fluorescent upright microscope after TCS exposure for 120 h (Fig. 3 F). Compared to the control group, the 125 and 250-μg/L TCS treatments significantly resulted in blood vessel ablation in head, including nasociliary artery, anterior cerebral artery, middle cerebral veins, dorsal longitudinal veins, posterior cerebral veins, central arteries, original brain-channel, and common cardinal veins, as well as the absence of subcutaneous veins and inner optic circle of eyes, and pericardial vascular defects. In the 62.5-μg/L treatment, the vascular development defects were not obvious for the trunk blood vessels, including intersegmental vessels (ISV), dorsal aorta (DA), posterior main vein (PCV). The ISV showed a typical "S" shape in the control group compared to an almost linear form in the TCS-exposure treatments. This indicates that the transverse spacing of ISV became shorter, and hematopoiesis was varicose and dysplasia under trunk. Especially, the transverse PCV of the trunk showed significant ablation in the 250-μg/L treatment (Fig. 3F). These findings offer strong evidence that TCS severely affected the development of neural and vascular networks, further contributing to abnormal behavior.

Apart from the developmental toxicity of blood vessels in larvae, TCS also restrained the development of hair cells and the lateral line neuromast system. Through SEM observation, we found that the development of hair cells and neuromast of L1-L6 was in good order, and hair cell bundles had many long stereocilia that were developmentally neat and dense in the control group (Fig. 3G). The hair cell bundles in the TCS-exposure groups were short, sparse and scattered and the basal plates of neuromast colliculus became small, distortional, sunken or swollen, and irregularly textured compared to the control group. By DASPEI specific staining, the number of hair cells were significantly reduced ($p < 0.01$) when exposed to TCS (Fig. 3H). To decipher the relationship between the aforementioned phenotype malformations and neurotransmission functions, the changes in AChE activities were also examined. As shown in Fig. 3I, the AChE activity in the 62.5-μg/L treatment was significantly higher ($p < 0.001$), whereas the 250-μg/L treatment was significantly decreased by more than 80% as compared to the control group ($p < 0.01$). Accordingly, these observations provide compelling evidence for neurobehavioral abnormalities caused by TCS exposure.

Neurobehavior and movement capacity are dominated by the expressions of multiple genes, especially those related to neural regulation and vascular formation. To disclose the regulation of nerve-related target genes targeted by miR-144 on the above symptoms, the 3′UTR region of target genes bound by miR-144 were elucidated (Fig. 4A). We used the ECR Browser (https://ecrbrowser.dcode.org/) (Threshold=0.7) to compare the sequence homology of candidate target genes between zebrafish and humans, and found that all these genes from zebrafish had high homology with humans, some reaching 100% (Fig. S1). Moreover, RT-qPCR analysis were conducted with these neuro-/vascular related target genes of miR-144 (Fig. 4B-H). With the increase of TCS exposure concentration, *cd*36, *syn*2a, *fli*1a and *kdr*1 were significantly down-expressed ($p < 0.05$ or $p < 0.01$), whereas the genes *gper*, *epas*1b and *dpf*2 were significantly up-expressed. The abnormal expressions of these functional genes contributed to the neurotoxicity induced by TCS exposure in zebrafish larvae. It can be inferred from the analysis that TCS exposure led to neurodevelopmental toxicity originating from the abnormal expressions of these genes targeted by miR-144.

3.4. Confirmation of neurodevelopment and neurobehavior regulation for miR-144 by intervened expression

Artificially intervened expression of miR-144 was achieved by microinjecting its agomir or antagomir at the 1–2 cell embryonic stage (Fig. 5A). Over-expression and knockdown of miR-144 were accomplished as in our previous report (Li et al., 2016; Ma et al., 2019). The microinjection of miR-144 mimics and inhibitors effectively interfered with the relative copy abundance of miR-144 in 120-hpi (hours post-injection) larvae when compared to the negative control (NC) ($p < 0.001$ or $p < 0.05$) (Fig. 5B). Both RT-qPCR and transcriptome sequencing data confirmed the up-regulation of miR-144 under TCS exposure (Fig. 2B). To this end, the embryos injected with miR-144-inhibitor were simultaneously exposed to 250-μg/L TCS to observe whether it would rescue/eliminate the over-expression of miR-144, and to verify that the neurotoxicity was induced by the up-regulation of miR-144 upon TCS exposure. As anticipated, the prominent rescue phenomenon was observed as compared to the individual miR-144 inhibitor (Fig. 5B).

Next, we used the Noldus behavioral analysis instrument to further track the abnormal behavior of larvae after over-expression or knockdown of miR-144. The motility of zebrafish larvae was normal and the trajectories were uniform in the negative control. After microinjection of miR-144 mimics and inhibitors, some larvae were hyperexcitable and rapidly moved circumferentially around the hole of the 96-well plates, however, more individuals didn't move at all, as was most significant for the miR-144 mimic group. In the miR-144 inhibitor+TCS group, the abnormal behavior of motion trajectory was alleviated (Fig. 5 C). These quantitative results showed that the average swimming distance and speed of 120-hpi larvae were significantly reduced after microinjection of miR-144 mimics and inhibitors ($p < 0.001$ or $p < 0.01$). Notably, the miR-144 inhibitor+TCS group showed a certain degree of rescue effect and no difference from the NC group (Fig. 5D).

In the light-dark rhythmic response test, the larval activities in the mimic and inhibitor groups were lower than those in the NC group and inhibitor+TCS group in the light environment. Notably, the movement speed of larvae in the mimic group showed almost no difference under light/dark alternation (Fig. 5E). Similarly, the response to acoustic stimulation in the mimic group was much smaller than that in the NC group (Fig. 5F), demonstrating ~~showing~~ that the locomotion rates of larval zebrafish were significantly reduced ($p < 0.001$). However, no significant difference was observed in the inhibitor and inhibitor +TCS groups ($p < 0.05$) versus the NC group. According to the above behavioral tracking experiments, we infer that the expression changes of miR-144 could cause abnormal behavior, in which the over-expression was more toxic than the corresponding knockdown.

To better understand the effect of miR-144 expression on neural and

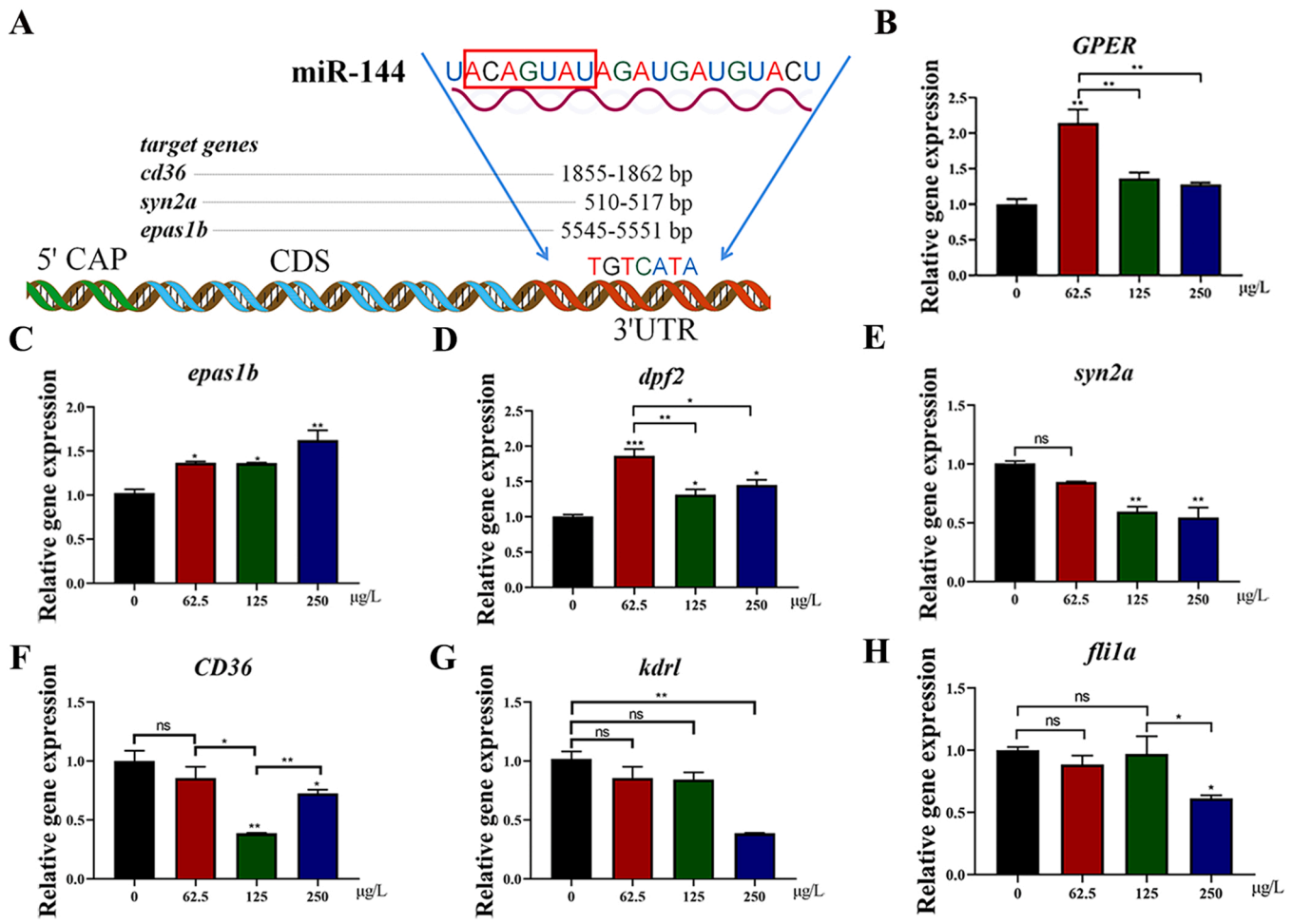

Fig. 4. The verification of target genes regulated by miR-144 and their expression changes under TCS exposure. Notes: (1) A, Schematic diagram of the 3′UTR region of GPER (target genes) bound by mir-144; (2) B-H, The expression changes of neural related genes targeted by miR-144; (3) All values were expressed as mean ± SD in triplicate (n = 3), "ns" means no significant difference, "*", "**" and "***" indicate significance levels at $p < 0.05$, $p < 0.01$ and $p < 0.001$, respectively.

vascular networks, we microinjected miR-144-mimic, inhibitor and NC into Tg (*fli*-1:EGFP) embryos at the 1–2-cell stage, and part of the embryos injected with inhibitor were exposed to 200-μg/L TCS. Blood vessel development was observed with a Nikon fluorescent upright microscope at the 120-hpi stage (Fig. 5G). Blood vessel ablation in the head, absence of subcutaneous veins, inner optic circle veins of eyes and pericardial vascular defect appeared in the mimic and inhibitor groups. As shown in Fig. 5G, the trunk blood vessels were observed in each treatment group. In the NC group, ISV showed a typical "S" shape, displaying the DA and transverse PCV of trunk to be clearly visible and consecutive. However, they all showed significant ablation, as well as blurred and indistinct phenomena in both mimic and inhibitor groups. The hematopoiesis under the trunk was also varicose and dysplasia. Notably, the vascular development in the inhibitor + TCS group was better than those of the mimic and inhibitor groups. The quantitative analysis of the vascular network also confirmed the aforementioned changing trend (Fig. 5H). Meanwhile, after miR-144 was over-expressed or knocked down, the vascular angiodysplasia triggered larval phenotypic malformations, such as spinal curvature, yolk edema, swimming sac defect and pericardial edema. Additionally, zebrafish malformation was alleviated in the inhibitor+TCS group (Fig. 5G). The collective evidence indicates that the abnormal expression of miR-144 is unfavorable for vascular development, and its over-expression is more harmful than its suppression, which is consistent with the toxic effects of miR-144 up-regulation under TCS exposure.

As shown in Fig. 5I, the development of hair cells and neuromast for 120-hpi larvae was observed after artificial intervention of miR-144 expression. By SEM observation, the hair bundles of neuromast appeared to be dense and long, and the basal plates of neuromast colliculus had regular folds and textures in the NC group. However, the neuromast hair cells in the mimic group were short, thin and scattered. In the inhibitor group, the hair bundles were also sparse and the basal plates of neuromast colliculus became distortional as compared to the NC group. Similarly, the development of hair cell and neuromast in the inhibitor+TCS group was close to their normal state. Based on DASPEI specific staining, the number of hair cells was significantly reduced under the intervened expression of miR-144 when compared to NC and blank control groups. In sharp contrast, the hair cells in the inhibitor+TCS group were significantly recovered. These observations provide compelling evidence that the abnormal expression of miR-144 can damage the zebrafish lateral line sensing system and neurodevelopment. Moreover, the activity of AChE was inhibited under abnormal expression of miR-144 ($p < 0.05$ or $p < 0.01$), whereas there were no differences with the NC and inhibitor+TCS groups (Fig. 5J).

Owing to the contribution of miR-144 to neurodevelopmental toxicity, we further explored how miR-144 induced these effects by regulating the functional genes related to neural and vascular differentiation. Changes in the expression of 7 target genes were confirmed by RT-qPCR after artificial intervention of miR-144. Firstly, the more probable genes targeted by miR-144 were *cd*36, *syn*2a and *epas*1b with high binding scores, which were demonstrated by the double luciferase analysis system according to Sun and coworkers (Sun et al., 2020)

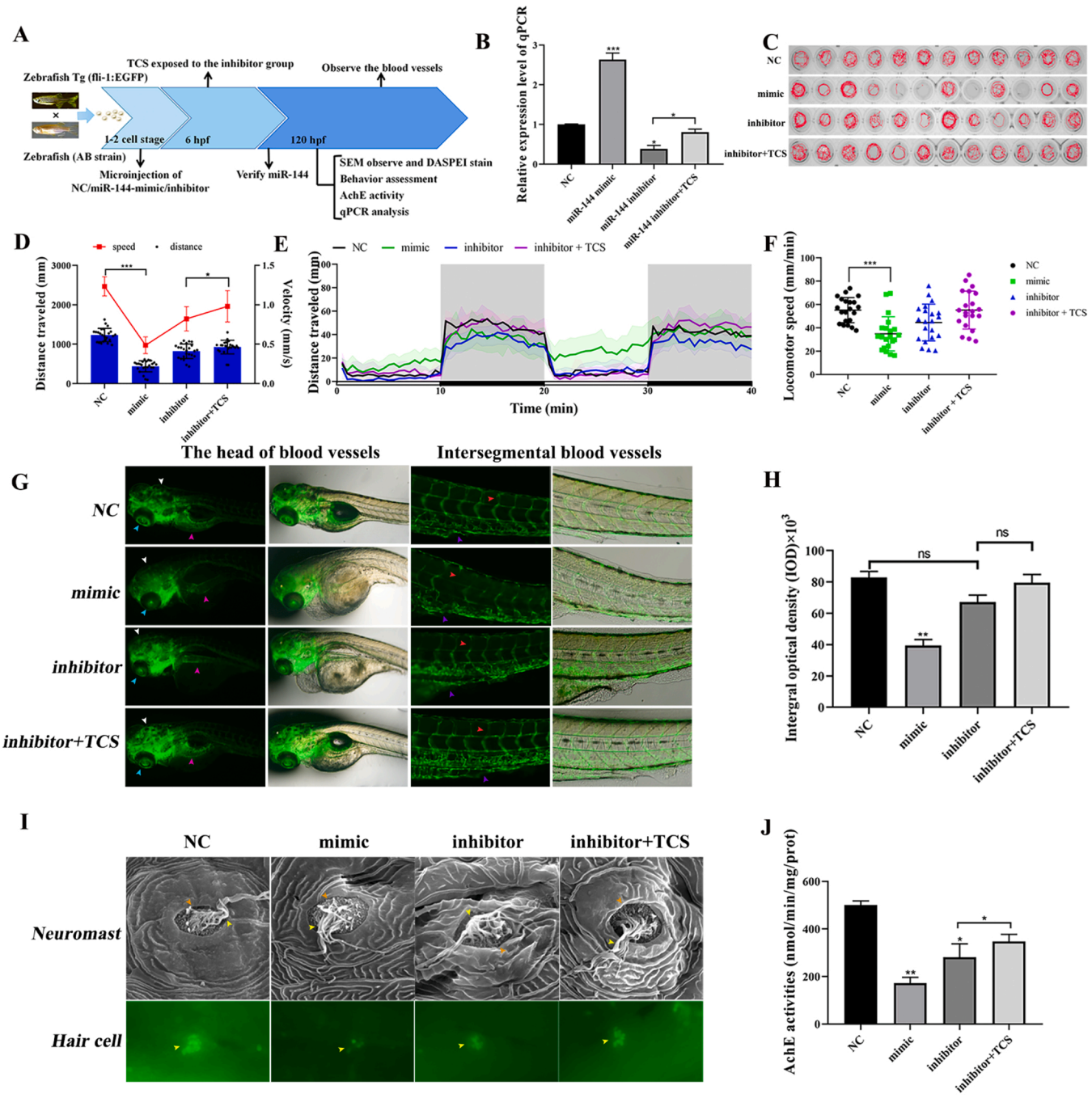

Fig. 5. The effects on neurodevelopment and neurobehavior of zebrafish larvae under artificial intervention expression of miR-144, Notes: (1) A, Experimental schematic illustration; (2) B, Validity confirmation of miR-144 overexpression and knockdown by RT-qPCR; (3) C, Autonomous motion trajectory capture of zebrafish larvae (120 hpi, hours post-injection) microinjected with of NC/miR-144-mimic/inhibitor for 20 min; (4) D, Quantitative analysis of swimming distance and average speed of zebrafish larvae (120 hpi); (5) E, Effects on light-dark rhythm of zebrafish larvae (120 hpi) injected with NC/miR-144-mimic/inhibitor; (6) F, Effects on acoustic stimulation response of zebrafish larvae (120 hpi) injected with NC/miR-144-mimic/inhibitor; (7) G, Effects on head (×40) and trunk (×200) blood vessel development of 120 hpi zebrafish larvae injected with NC/miR-144-mimic/inhibitor (Left: dark field shooting, Right: bright and dark field merged); (8) H, Effects on the neuromast development by scanning electron microscopy and the hair cells differentiation by DASPEI-staining in 120 hpi zebrafish larvae; (9) I, Quantitative analysis of hair cell number in 120 hpi zebrafish larvae; (10) J, Effect of on the activity of AChE in zebrafish larvae (120 hpi); (11) White arrows point to dorsal longitudinal vein (DLV), light blue arrows point to inner optic circle (IOC), purple arrows point to branchial artery, red arrows point to intersegmental vessels (ISVs), dark blue arrows point to posterior cardinal vein (PCV), orange arrows point to the L1 neuromast and yellow arrows point to L1 neuromast hair bundles; (12) All values were expressed as mean ± SD in triplicate (n = 3), "ns" means no significant difference, "*", "**" and "***" indicate significance levels at $p < 0.05$, $p < 0.01$ and $p < 0.001$, respectively.

(Fig. 6 A). We found that the luciferase activity was significantly inhibited ($p < 0.001$) in 48-hpi embryos injected by miR-144 mimics, whereas the luciferase activities of pGL0-wt and pGL0-mut showed no significant difference in comparison with the negative control ($p < 0.05$) (Fig. 6B). These results demonstrate that miR-144 can reversely regulate the expression of *cd*36, *syn*2a and *epas*1b by binding to their 3 '-UTR, that is, *cd*36, *syn*2a and *epas*1b were verified to be the target genes of miR-144. By RT-qPCR, the expressions of *cd*36, *syn*2a, *epas*1b and *fli*-1a

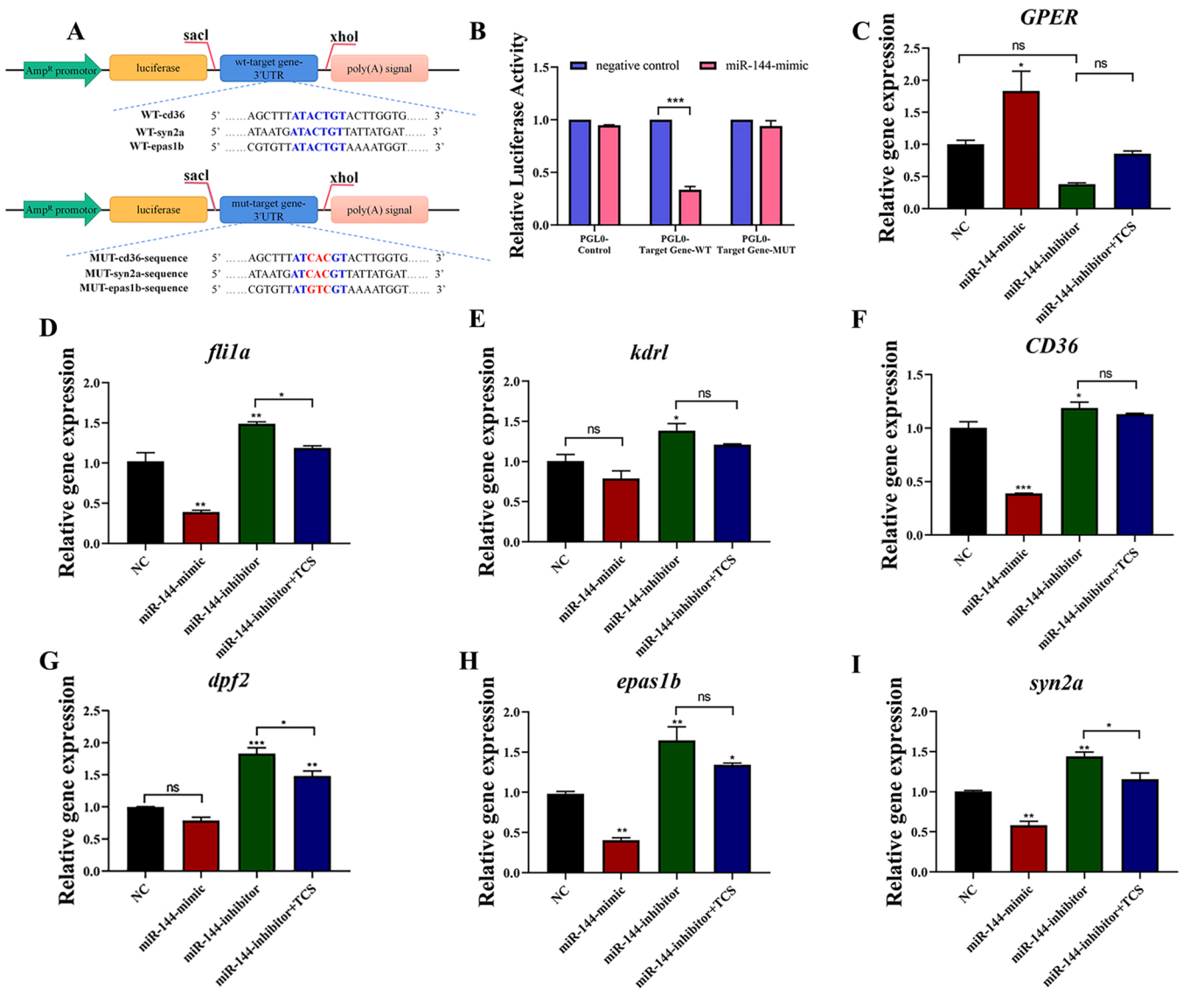

Fig. 6. The expression changes of target genes under miR-144-overexpression/knock down, Notes: (1) A, Vector construction diagram of double luciferase analysis system of target genes 3′ -UTR; (2) B, Double luciferase activity assay in zebrafish embryo after injection of the constructed vectors; (3) C-I, Target gene expression after miR-144-overexpression/knock down; (4) All values were expressed as mean ± SD in triplicate (n = 3), "ns" means no significant difference, "*", "**" and "***" indicate significance levels at $p < 0.05$, $p < 0.01$ and $p < 0.001$, respectively.

were prominently down-regulated ($p < 0.01$ or $p < 0.001$), whereas those of *kdr*l and *dpf*2 were slightly inhibited with no significant difference ($p < 0.05$) after microinjection of miR-144 mimics. Except for *gper* up-regulation, the expressions of the other six target genes were all down-regulated in the treatment group receiving microinjection of miR-144 inhibitor ($p < 0.05$, $p < 0.01$ or $p < 0.001$). The miR-144 inhibitor+TCS-exposure group decreased the over-expression of these genes to a certain degree (Fig. 6C-I). Based on the above analysis and in accordance of previous literature, we posit that the up-regulation of miR-144 induced neurotoxicity by targeting functional genes related to neural and vascular development.

3.5. Activation of the PKC/MAPK pathway triggers miR-144 up-regulation

Based on KEGG enrichment analysis, the miR-144-regulated target genes were concentrated in the MAPK pathway (Fig. 1E). A large number of studies confirmed that the MAPK signaling pathway had a regulatory effect on the CNS and hair cell development (Fig. S2) (Liu et al., 2021). Many neurological diseases are accompanied by activation or inhibition of the PKC/MAPK signaling pathway, such as autism spectrum disorder (ASD), Parkinson's disease (PD), etc. (Li et al., 2020; Zhu et al., 2020). Thus, we posit that TCS targets GPER for activation of the PKC/MAPK signaling pathway, in which PKC is phosphorylated to become dissociated from the PKC-Keap1 compound and thereby becomes activated (Huang et al., 2020). MAPK is mainly composed of four sub-families, which are extracellular signal-regulated kinase (ERK), p38 mitogen-activated protein kinase (p38 MAPK), c-Jun N-terminal kinase (JNK) and extracellular signal-regulated kinase 5 (ERK5) (Dou et al., 2021). An overall conceptual representation is elaborated in Fig. 7A for the sake of elucidating the above conjecture. Firstly, the expression changes of key genes in the PKC/MAPK signaling pathway were detected by RT-qPCR under exposure to gradient concentrations of TCS (Fig. 7B-H). Table S4 lists the specific primer sequences for these genes. With increasing TCS concentrations, the expressions of *PKC,* located at the upstream, and nuclear transcription factor *jun*D and *SRFα*, located at the downstream of PKC/MAPK pathway, were both significantly up-regulated ($p < 0.05$, $p < 0.01$ or $p < 0.001$). Conversely, the

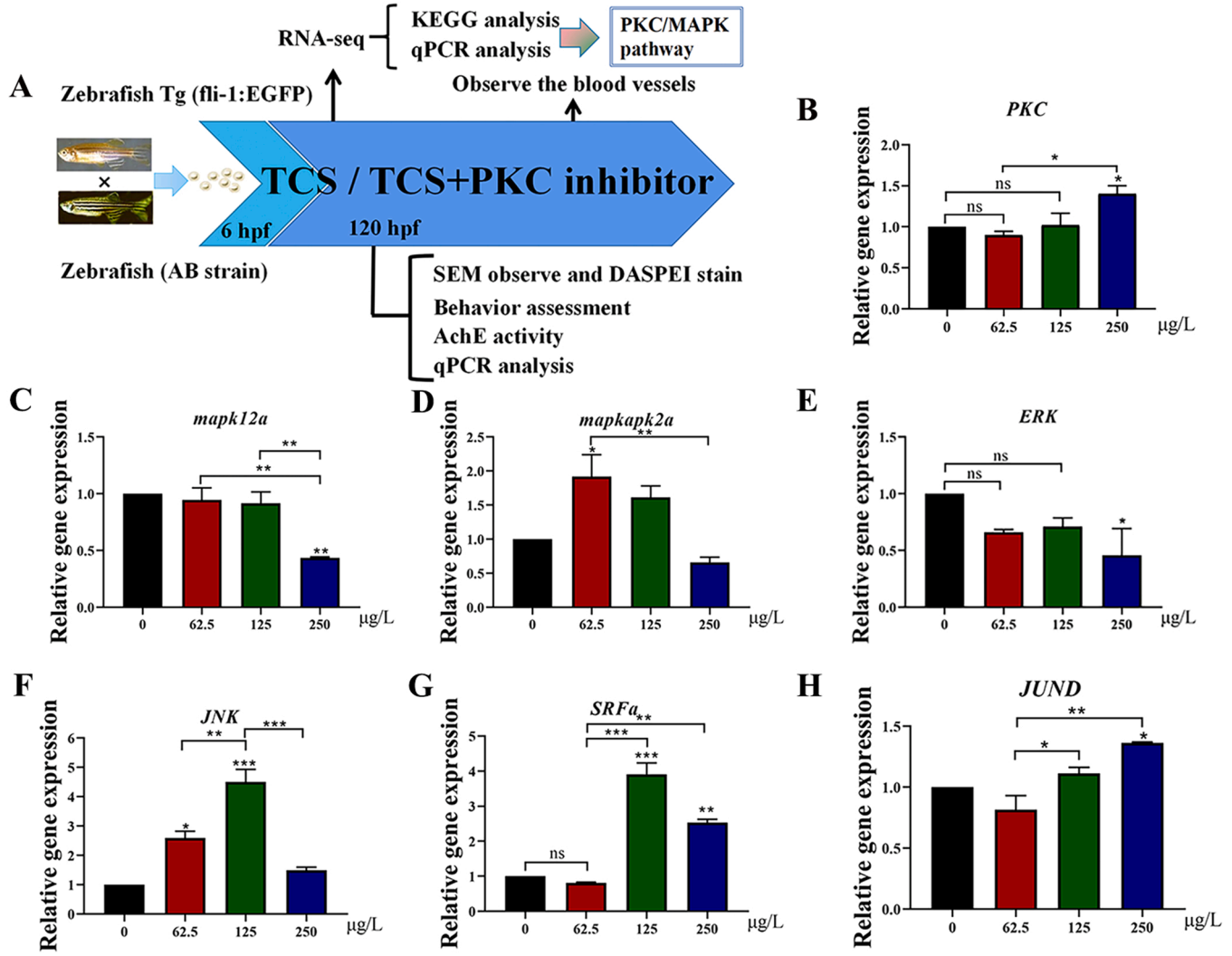

Fig. 7. The expression changes of key genes in PKC / MAPK signaling pathway under TCS exposure, Notes: (1) A, Experimental schematic diagram; (2) B-H, under TCS exposure, qPCR verifies the expression changes of PKC, mapk12a, mapkapk2a, ERK, JNK, SRFα and JUND genes in the PKC/MAPK signaling pathway and (3) All values were expressed as mean ± SD in triplicate (n = 3) "ns" means no significant difference, "*", "**" and "*** " indicate significance levels at $p < 0.05$, $p < 0.01$ and $p < 0.001$, respectively.

expression of ERK was significantly down-regulated. The expressions of *mapkl*2a, *mapkapk*2 and *JNK* were increased in the 62.5-μg/L treatment ($p < 0.05$, $p < 0.01$ & $p < 0.001$) and slightly reduced in the 250-μg/L treatment (Fig. 7B-H). The above-mentioned genes participate in different functions, such as ERK's regulation of cell growth and differentiation. JNK and p38 MAPK signaling pathways play important roles in stress responses to inflammation and apoptosis, and their activation will further activate the downstream molecules that promote apoptosis (Coulthard et al., 2009). The expression changes of marker genes in the PKC/MAPK signaling pathway hint that TCS activates GPER and further triggers the activation of this pathway.

To document the up-regulation of miR-144 resulting from the activation of the PKC/MAPK signaling pathway, we suppressed the activity of the PKC/MAPK signaling pathway by employing MTO, quantified the expression of miR-144 and evaluated the rescue/recovery effects under TCS exposure. As an inhibitor of topoisomerase II, MTO can suppress the activity of protein kinase C (PKC). Since 20% of MTO's IC_{50} (8.5 μM) was sufficient for inhibiting PKC, the MTO concentration was set to 1.7 μM for subsequent experiments trials. In the compound treatment of MTO+TCS, the expression changes of key genes in the PKC/MAPK signaling pathway were effectively inhibited as expected after using MTO ($p < 0.05$, $p < 0.01$ & $p < 0.001$) (Fig. 8A). The expression of miR-144 at the downstream PKC/MAPK signaling pathway was significantly down-regulated compared to the sole TCS-exposure treatment (Fig. 8B). Moreover, the expression changes for miR-144 target genes related to neurotoxicity and vascular development showed an opposite trend in the MTO+TCS treatment as opposed to the TCS-exposure treatment (Fig. 8 C). As expected, TCS induced neurodevelopmental toxicity by targeting GPER and then activating the PKC/MAPK pathway.

To demonstrate the effects of MTO on zebrafish development and behavior, we tracked the autonomous movement of 120-hpf larvae exposed to TCS or MTO+TCS for 20 min (Fig. 8D-E). The larval swimming speed and distance were significantly increased in the MTO+TCS (200 μg/L) treatment as compared to the TCS treatment ($p < 0.001$). Larval behavior was restored and rescued in the light-dark transition rhythms, and also the sensitivity to acoustic stimulation was improved in the MTO+TCS treatment group ($p < 0.05$) (Fig. 8F-G). As illustrated in Fig. 8H, the blood vessel networks in head, the subcutaneous veins and veins of the inner optic circle of eyes were restored, and the developmental malformations were alleviated in the presence of MTO.

To further unravel the regulation of the PKC/MAPK signaling pathway on zebrafish lateral line neural system development, SEM and DASPEI staining were used to observe the development of larval neuromast and hair cells. Similarly, the developmental morphology of the

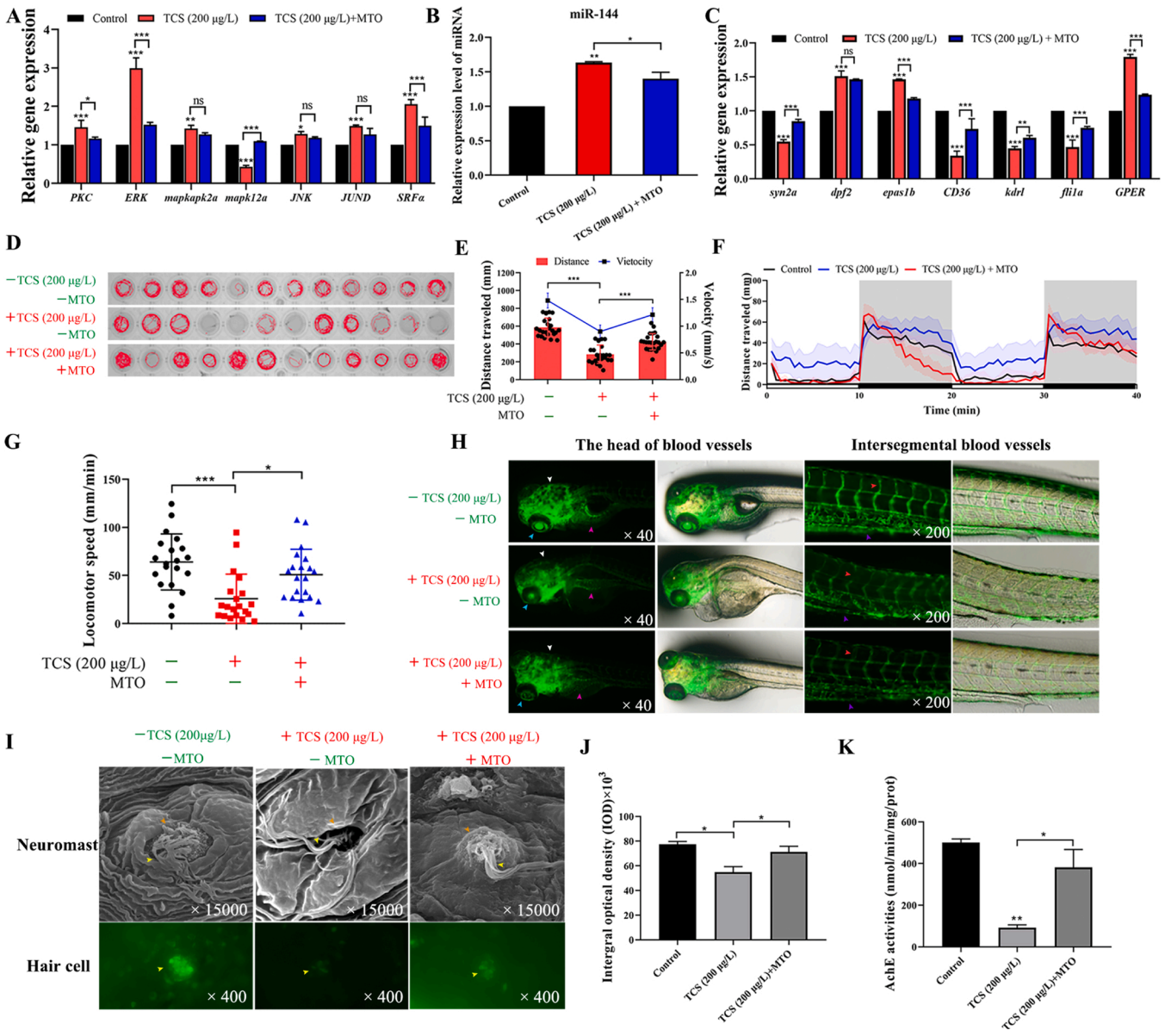

Fig. 8. TCS exposure induces neurodevelopmental toxicity by activating PKC/MAPK pathway, Notes: (1) A, After adding a PKC inhibitor, the expression of key genes in the PKC/MAPK signaling pathway; (2) B, After adding a PKC inhibitor, the expression of miR-144; (3) C,After adding a PKC inhibitor, the expression of target genes regulated by miR-144; (4) D, Autonomous motion trajectory capture of zebrafish larvae (120hpf) for 20 min using PKC/MAPK pathway inhibitor (MTO) compared with TCS exposure; (5) E, Quantitative analysis of swimming distance and average speed of zebrafish larvae (120 hpf) using TCS/ TCS + MTO treatments; (6) F, Effects on light-dark rhythm of zebrafish larvae (120 hpf) for 20 min using TCS/TCS + MTO treatments; (7) G, Effects on acoustic stimulation response of zebrafish larvae (120 hpf) for 40 min using TCS/TCS + MTO treatments (samples, 3 ×32); (8) H, Effects on head (×40) and trunk (×200) blood vessel development of 120 hpf zebrafish larvae using TCS/TCS + MTO treatments (samples, 3 ×12) (Left: dark field shooting, Right: bright and dark field merged); (9) I, Effects on the neuromast development by scanning electron microscopy and the hair cells differentiation by DASPEI-staining in 120 hpf zebrafish larvae using TCS/TCS + MTO treatments (samples, 3 ×12); (10) J, Quantitative analysis of hair cell number in 120 hpf zebrafish larvae; (11) K, Effect of on the activity of AChE in zebrafish larvae (120 hpf) using TCS/TCS + MTO treatments; (12) White arrows point to dorsal longitudinal vein (DLV), light blue arrows point to inner optic circle (IOC), purple arrows point to branchial artery, red arrows point to intersegmental vessels (ISVs), dark blue arrows point to posterior cardinal vein (PCV), orange arrows point to the L1 neuromast and yellow arrows point to L1 neuromast hair bundles; (13) All values were expressed as mean ± SD in triplicate (n = 3), "ns" means no significant difference, "* ", "* *" and "* ** " indicate significance levels at $p < 0.05$, $p < 0.01$ and $p < 0.001$, respectively.

neuromast, stereocilia bundle and number of hair cells were all restored to almost their normal states ($p < 0.05$) under the combined action of TCS and MTO (Fig. 8 F). Compared to the TCS-exposure treatment, AChE was significantly activated in the compound treatment ($p < 0.05$, Fig. 8I). The increased AChE activity in the MTO+TCS treatment confirmed that MTO rescued the inhibitory effect of TCS exposure on neurotransmitter transmission, further providing an explanation for the as-described behavior abnormality. All of these behavioral tracking experiments offer strong evidence for our conjecture that TCS induces neurotoxicity by way of activation of the PKC/MAPK signaling pathway.

4. Discussion

We used zebrafish as a model organism to explore the underlying molecular mechanisms regarding TCS induced neurotoxicity, given that they have mammalian-like nervous systems, which are relatively simple and accessible. To characterize the neurotoxic effects of TCS exposure, we evaluated that related response indicators, which included

behavioral analysis, vascular and lateral line system development, AChE activity, and RT-qPCR of neuro/vascular-related functional genes. The motor behavior of zebrafish clearly reflects the developmental integrity of the zebrafish nervous system, whereby light/dark and sound stimuli can be used to probe the perception ability of zebrafish to their surrounding environment. Vascular and neural networks cross-talk as the cranial vasculature governs the neurobehavior and development of the CNS, and the intersegmental artery provides nutrient and metabolite transport for all tissues (Khor et al., 2016). Concurrently, zebrafish rely on the neuromast in the lateral line system to detect water flow, water temperature and detect environmental signals, contributing to predation food, defense and protection against danger, leaning, reproductive behavior and so on (Bleckmann and Zelick, 2009; Suli et al., 2016). AChE is key indicator to ensure the normal transmission of nerve signals in the organism owing to its central role in the nerve conduction of cholinergic synapses. AChE can degrade acetylcholine and inhibit the excitatory effect of neurotransmitter on the postsynaptic membrane (Oliveira Santos and Leal Rato, 2021). In our investigation, TCS exposure triggered abnormal circadian rhythm, movement behavior and blood vessel development, as well as reduced hair cells and injured neurotransmitter conduction in zebrafish larvae.

To explore the mechanism of neurotoxicity induced by TCS, we combined RNA sequencing data with relevant information from previous studies to screen out functional genes (*gper*, *epas1b*, *dpf2*, *syn2a*, *cd36*, *kdr1*, and *fli1a*) participating in neurodevelopment, neurotransmitter transmission and vascular angiogenesis, as subsequently validated with RT-qPCR. *GPER* is widely distributed throughout the cardiovascular system and CNS, and affects the transmission of neurotransmitters and the generation of neurons (Xu et al., 2017, 2021). The functions of *epas1b* and *syn2a* are related to neural differentiation and neurotransmitter transmission, respectively, and both are considered sensitive marker genes for neurodevelopment. *dpf2* was related to the development of the nervous system, and heterozygous mutations in the *dpf2* gene can lead to Coffin-Siris syndrome (Saviola et al., 2021). *CD36* protein is a cell surface glycoprotein that is known to promote endothelial cell angiogenesis, and its lack of endothelial cells prevents normal angiogenesis and vascular repair (Bou Khzam et al., 2020). The down-regulation of *Kdr1* can cause defects in embryonic angiogenesis (Shin et al., 2016), and *Fli-1* is a marker gene related to cardiovascular formation (Nakamura et al., 2020). The abnormal expression of the above genes following TCS exposure indicated a linkage between TCS exposure and developmental neurotoxicity that affects angiogenesis, vascular repair, neural differentiation and neurotransmitter transmission.

Through sequencing and bioinformatics analysis, we screened out miR-144, which significantly over-expressed in the TCS-exposure treatments compared to the control group. Overexpression and knockdown of miR-144 caused neurotoxicity and behavioral abnormalities in zebrafish larvae, especially in the over-expressed case. With respect to miR-144 regulatory genes, only *gper* was up-regulated, which exhibited an opposite expression compared to other genes.We previously demonstrated by WISH analysis that *gper* expression in the CNS of 5-dpf larvae was significantly enhanced when exposed to high concentrations of TCS (Wang et al., 2020). This resulted in a significant up-regulation for miR-144 expression in our study. After the injection of miR-144 mimic, a similar up-regulation of *gper* was obtained, but this finding was inconsistent with the mechanism by which miRNAs bound 3′-UTR to repress target genes. Based on the TargetScan prediction, the binding score (67) for miR-144 to GPER was relatively low, leading to an up-regulated expression of GPER concomitant with theactivation of miR-144 (Fig. 2 C). Moreover, the JASPAR web analysis confirmed, JUND as a transcription factor with a high predictive score for GPER (Huang et al., 2020). The target genes of miR-144 are related to the MAPK pathway; for example, both *mapk12a* and *mapkapk2a* are not only the target genes of miR-144, but also key genes in the MAPK signaling pathway. Consequently, we infer that the over-expression of miR-144 and activation of the MAPK signaling pathway restrict each other, and the transcription factor JUND participates in the transcription process of GPER.

By KEGG enrichment analysis, miR-144 was predicted to influence the MAPK signaling pathway. TCS acts on GPER and activates the hydrolysis of PLC and PIP2 to produce DAG, whose kinase activates PKC to trigger physiological effects and enhance intracellular pH and Ca^{2+} level (Williams, 2019). PKC is an upstream signaling molecule of the MAPK signaling pathway, the activation of which plays crucial roles in regulating the expressions of neurodevelopment-related genes and the growth of proto-oncogenes. The negative feedback mechanisms on the PKC/MAPK signaling pathway are controlled by PKC in cell-signal transduction procedures (Li et al., 2021). When the PKC is activated, various downstream protein kinases will be subsequently stimulated, especially MAPK that has a regulatory function of cell growth. MAPK plays a key role in transmitting cellular signals and usually constitutes a multi-layered pathway for many kinds of kinases, such as ERK, p38 MAPK, JNK and ERK5. The signaling transduction pathways that the aforementioned kinases take part in possess varying functions, such as a regulatory roles for ERK in the growth and differentiation of cells and the involvement of JNK and p38 MAPK in crucial process retarding the incidence of cellular inflammation and apoptosis (Li et al., 2021). The activated MAPK pathway promotes the phosphorylation of certain amino acid residues from many transcription factors in the cytoplasm, such as JUN, SRF, etc., to activate the nuclear transcription factors, and promote/regulate gene expressions (Fig. 9A and Fig. S2). Building upon the above research findings, we used PKC inhibitor MTO to investigate a series of neurotoxicity indicators and key genes for the signaling pathway. Accordingly, the PKC/MAPK signaling pathway was demonstrated to be involved in TCS-induced zebrafish neurotoxicity. Through the JASPAR website, we found several high-scoring transcription factors JUND, SRF, GABPA and LIN54 for pri-mir-144 (Fig. 9B), among which the JUND and SRF were confirmed to be activated by ERK and JNK, respectively. The inhibited activity of PKC was concomitant with the significantly reduced expression of miR-144, highlighting the participation of PKC in the upstream signaling transduction process of miR-144.

Herein, the relationship between TCS and GPER was determined from the perspective of miRNA. In addition to causing neurological disorder, TCS acts on miR-144 to induce an estrogenic effect by GPER activation. In our investigation, the use of the pathway inhibitor MTO to suppress the expression of the upstream signaling molecule PKC in the PKC/MAPK pathway simultaneously triggered the inhibition of downstream transcription factor JUND and the decrease of GPER expression, which were consistent with previous results (Huang et al., 2020). Collectively, this findings infer that the TCS-induced neurotoxicity was attributed to the abnormal expression of miR-144 mediated by activation of the PKC/MAPK signaling pathway. However, as a new type of estrogen receptor, further research is necessary to document the similarities and differences between GPER and classical nuclear receptor in organisms, as well as its underlying functions and molecular mechanisms.

5. Conclusions

In this study, Illumina miRNA-seq analysis identified four common positively differentiated miRNAs resulting from TCS exposure to zebrafish larvae. The expression distribution and functional analysis of positively differentiated miRNAs showed that they were directly or indirectly involved in neurodevelopment and neurobehavior. Notably, miR-144 up-regulation caused vascular malformation, and severely affected hair cell development and formation of the lateral line neuromast system, thereby leading to abnormal motor behavior. Through intervening in the expression of miR-144 by microinjection of its mimics and inhibitors to 1–2-cell embryos, we acquired similar phenotypic malformations and neurobehavioral abnormalities to those induced by

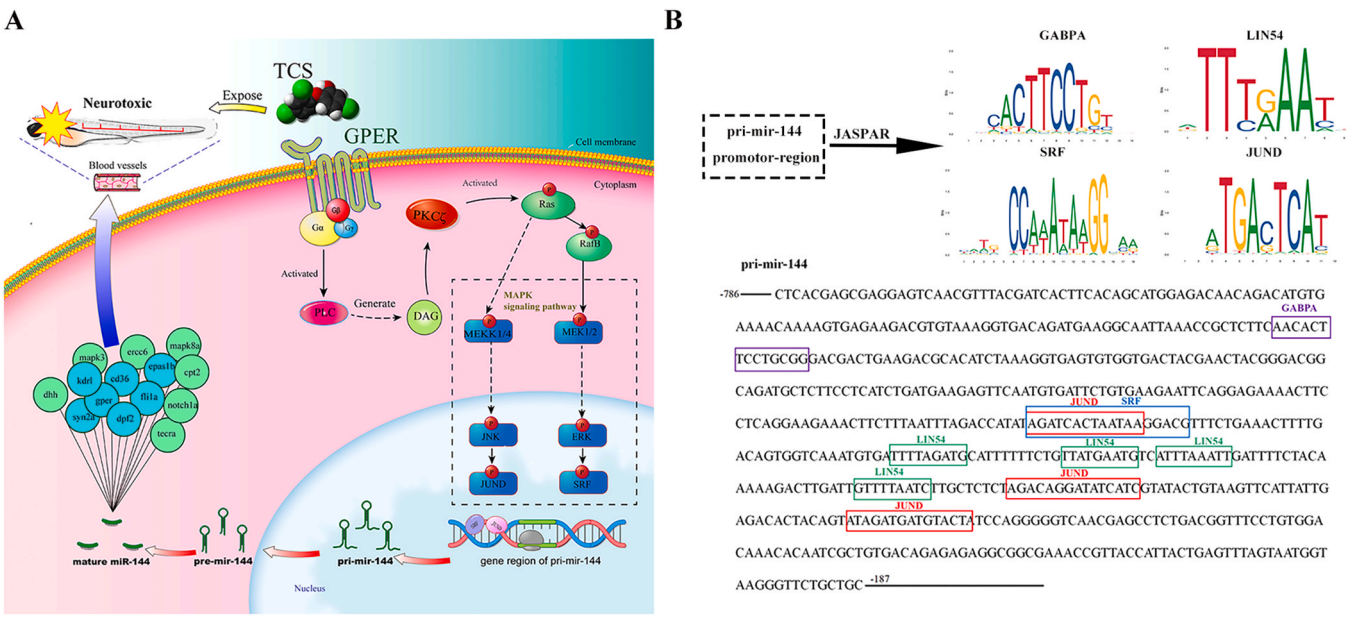

Fig. 9. The analysis of potential regulatory mechanism of TCS-induced neurotoxicity in zebrafish, Notes: (1) A, The mechanism of TCS targeting GPER through PKC/MAPK signaling pathway to induce neurotoxicity in zebrafish larvae; (2) B, Prediction scheme of transcription factor and the binding sites for transcription factors are in box; (3) Red font for JUND binding site, purple font for GABPA, blue font for SRF, green font for LIN54.

TCS neurotoxicity, such as vascular developmental malformation, impaired lateral line neuromast system development, and abnormal motor behavior. The changing trends for miR-144 target genes (*cd36*, *syn2a*, *epas1b*, *dpf2*, *fli1a* and *kdrl*) demonstrated that TCS exposure led to neurodevelopmental toxicity originating from abnormal expression of these genes targeted by miR-144. Up-regulation of miR-144 was attributed to activation of its upstream PKC/MAPK pathway by TCS-targeted GPER, which was further substantiated using MTO as a PKC inhibitor.

CRediT authorship contribution statement

Wenqi Diao: Conceptualization, Methodology, Data curation, Writing – original draft. **Qiuhui Qian**: Writing – review & editing. **Guangyao Sheng**: Visualization, Investigation, Supervision. **Anfei He**: Visualization, Investigation, Supervision. **Jin Yan**: Visualization, Investigation, Supervision. **Randy A. Dahlgren**: Correction in English expression. **Xuedong Wang**: Visualization, Investigation, Supervision. **HuiliWang**: Visualization, Investigation, Supervision.

Declaration of Competing Interest

The authors declare that they have no known competing financial interests or personal relationships that could have appeared to influence the work reported in this paper.

Acknowledgement

This work was jointly supported by the National Natural Science Foundation of China (32071617 and 31770552), China; Natural Science Foundation of Jiangsu Province (BK20191455), China; Entrepreneurship and Innovation Program of Jiangsu Province (Project No. 2018-2017), China; and Suzhou Municipal Science and Technology Project (SS2021150), China.

Appendix A. Supporting information

Supplementary data associated with this article can be found in the online version at doi:10.1016/j.jhazmat.2022.128560.

References

Bedoux, G., Roig, B., Thomas, O., Dupont, V., Le Bot, B., 2012. Occurrence and toxicity of antimicrobial triclosan and by-products in the environment. Environ. Sci. Pollut. Res. Int. 19, 1044–1065.
Bianchi, N., Zuccato, C., Finotti, A., Lampronti, I., Borgatti, M., Gambari, R., 2012. Involvement of miRNA in erythroid differentiation. Epigenomics 4, 51–65.
Bleckmann, H., Zelick, R., 2009. Lateral line system of fish. Integr. Zool. 4, 13–25.
Bou Khzam, L., Son, N.H., Mullick, A.E., Abumrad, N.A., Goldberg, I.J., 2020. Endothelial cell CD36 deficiency prevents normal angiogenesis and vascular repair. Am. J. Transl. Res 12, 7737–7761.
Cansız, D., Ustundag, U.V., Unal, I., Alturfan, A.A., Emekli-Alturfan, E., 2021. Morphine attenuates neurotoxic effects of MPTP in zebrafish embryos by regulating oxidant/antioxidant balance and acetylcholinesterase activity. Drug Chem. Toxicol. 1–9.
Coulthard, L.R., White, D.E., Jones, D.L., McDermott, M.F., Burchill, S.A., 2009. p38 (MAPK): stress responses from molecular mechanisms to therapeutics. Trends Mol. Med. 15, 369–379.
Delov, V., Muth-Köhne, E., Schäfers, C., Fenske, M., 2014. Transgenic fluorescent zebrafish Tg(fli1:EGFP)y[1] for the identification of vasotoxicity within the zFET. Aquat. Toxicol. 150, 189–200.
Dhillon, G.S., Kaur, S., Pulicharla, R., Brar, S.K., Cledón, M., Verma, M., Surampalli, R.Y., 2015. Triclosan: current status, occurrence, environmental risks and bioaccumulation potential. Int. J. Environ. Res. Public Health 12, 5657–5684.
Dou, B., Li, Y., Ma, J., Xu, Z., Fan, W., Tian, L., Chen, Z., Li, N., Gong, Y., Lyu, Z., Fang, Y., Liu, Y., Xu, Y., Wang, S., Chen, B., Guo, Y., Guo, Y., Lin, X., 2021. Role of neuroimmune crosstalk in mediating the anti-inflammatory and analgesic effects of acupuncture on inflammatory pain. Front. Neurosci. 15, 695670.
Fu, Y.F., Du, T.T., Dong, M., Zhu, K.Y., Jing, C.B., Zhang, Y., Wang, L., Fan, H.B., Chen, Y., Jin, Y., Yue, G.P., Chen, S.J., Chen, Z., Huang, Q.H., Jing, Q., Deng, M., Liu, T.X., 2009. Mir-144 selectively regulates embryonic alpha-hemoglobin synthesis during primitive erythropoiesis. Blood 113, 1340–1349.
Huang, W., Ai, W., Lin, W., Fang, F., Wang, X., Huang, H., Dahlgren, R.A., Wang, H., 2020. Identification of receptors for eight endocrine disrupting chemicals and their underlying mechanisms using zebrafish as a model organism. Ecotoxicol. Environ. Saf. 204, 111068.
Ishibashi, H., Matsumura, N., Hirano, M., Matsuoka, M., Shiratsuchi, H., Ishibashi, Y., Takao, Y., Arizono, K., 2004. Effects of triclosan on the early life stages and reproduction of medaka *Oryzias latipes* and induction of hepatic vitellogenin. Aquat. Toxicol. 67, 167–179.
Jagini, S., Konda, S., Bhagawan, D., Himabindu, V., 2019. Emerging contaminant (triclosan) identification and its treatment: a review. SN Appl. Sci. 1, 640.
Katsuura, S., Kuwano, Y., Yamagishi, N., Kurokawa, K., Kajita, K., Akaike, Y., Nishida, K., Masuda, K., Tanahashi, T., Rokutan, K., 2012. MicroRNAs miR-144/144* and miR-16 in peripheral blood are potential biomarkers for naturalistic stress in healthy Japanese medical students. Neurosci. Lett. 516, 79–84.
Khor, E.S., Noor, S.M., Wong, P.F., 2016. Expression of zTOR-associated microRNAs in zebrafish embryo treated with rapamycin. Life Sci. 150, 67–75.
Kumar, N.S., Soma, D.S., Kumar, M.S., 2018. Triclosan-an antibacterial compound in water, sediment and fish of River Gomti, India. Int. J. Environ. Health Res. 28, 461–470.

Li, J., Liu, J., Zhang, Y., Wang, X., Li, W., Zhang, H., Wang, H., 2016. Screening on the differentially expressed miRNAs in zebrafish (*Danio rerio*) exposed to trace β-diketone antibiotics and their related functions. Aquat. Toxicol. 178, 21–38.

Li, L., Wu, X.H., Zhao, X.J., Xu, L., Pan, C.L., Zhang, Z.Y., 2020. Zerumbone ameliorates behavioral impairments and neuropathology in transgenic APP/PS1 mice by suppressing MAPK signaling. J. Neuroinflamm. 17, 61–72.

Li, X., Pan, J., Wei, Y., Ni, L., Xu, B., Deng, Y., Yang, T., Liu, W., 2021. Mechanisms of oxidative stress in methylmercury-induced neurodevelopmental toxicity. Neurotoxicology 85, 33–46.

Li, Y., Zhao, Y., Cheng, M., Qiao, Y., Wang, Y., Xiong, W., Yue, W., 2018. Suppression of microRNA-144-3p attenuates oxygen-glucose deprivation/reoxygenation-induced neuronal injury by promoting Brg1/Nrf2/ARE signaling. J. Biochem. Mol. Toxicol. 32, e22044.

Ling, Y., Sun, L., Wang, D., Jiang, J., Sun, W., Ai, W., Wang, X., Wang, H., 2020. Triclosan induces zebrafish neurotoxicity by abnormal expression of miR-219 targeting oligodendrocyte differentiation of central nervous system. Arch. Toxicol. 94, 857–871.

Liu, L., Wang, S., Chen, R., Wu, Y., Zhang, B., Huang, S., Zhang, J., Xiao, F., Wang, M., Liang, Y., 2012. Myc induced miR-144/451 contributes to the acquired imatinib resistance in chronic myelogenous leukemia cell K562. Biochem. Biophys. Res. Commun. 425, 368–373.

Liu, Y., Wei, M., Mao, X., Chen, T., Lin, P., Wang, W., 2021. Key signaling pathways regulate the development and survival of auditory hair cells. Neural Plast. 2021, 5522717 https://doi.org/10.1155/2021/5522717.

Ma, Y., Zang, L., Wang, D., Jiang, J., Wang, C., Wang, X., Fang, F., Wang, H., 2019. Effects of miR-181a-5p abnormal expression on zebrafish (*Danio rerio*) vascular development following triclosan exposure. Chemosphere 223, 523–535.

Mufson, E.J., He, B., Nadeem, M., Perez, S.E., Counts, S.E., Leurgans, S., Fritz, J., Lah, J., Ginsberg, S.D., Wuu, J., Scheff, S.W., 2012. Hippocampal proNGF signaling pathways and β-amyloid levels in mild cognitive impairment and Alzheimer disease. J. Neuropathol. Exp. Neurol. 71, 1018–1029.

Nakamura, K., Taniguchi, T., Hirabayashi, M., Yamashita, T., Saigusa, R., Miura, S., Takahashi, T., Toyama, T., Ichimura, Y., Yoshizaki, A., Trojanowska, M., Fujiu, K., Nagai, R., Sato, S., Asano, Y., 2020. Altered properties of endothelial cells and mesenchymal stem cells underlying the development of scleroderma-like vasculopathy in KLF5;Fli-1 mice. Arthritis Rheumatol. 72, 2136–2146.

Oliveira Santos, M., Leal Rato, M., 2021. Neurology of the acute hepatic porphyrias. J. Neurol. Sci. 428, 117605.

Orvos, D.R., Versteeg, D.J., Inauen, J., Capdevielle, M., Rothenstein, A., Cunningham, V., 2002. Aquatic toxicity of triclosan. Environ. Toxicol. Chem. 21, 1338–1349.

Rettberg, J.R., Yao, J., Brinton, R.D., 2014. Estrogen: a master regulator of bioenergetic systems in the brain and body. Front. Neuroendocr. 35, 8–30.

Saviola, D., De Gaetano, K., Galvani, R., Bosetti, S., Abbati, P., Igharo, V., De Tanti, A., 2021. Rehabilitation in a rare case of coffin-siris syndrome with major cognitive and behavioural disorders. J. Pedia Rehabil. Med. 14, 525–532.

Schultz, M.M., Bartell, S.E., Schoenfuss, H.L., 2012. Effects of triclosan and triclocarban, two ubiquitous environmental contaminants, on anatomy, physiology, and behavior of the fathead minnow (*Pimephales promelas*). Arch. Environ. Contam. Toxicol. 63, 114–124.

Shimozaki, K., 2021. Involvement of nuclear receptor REV-ERBβ in formation of neurites and proliferation of cultured adult neural stem cells. Cell Mol. Neurobiol. 41, 1611.

Shin, M., Beane, T.J., Quillien, A., Male, I., Zhu, L.J., Lawson, N.D., 2016. Vegfa signals through ERK to promote angiogenesis, but not artery differentiation. Development 143, 3796–3805.

Silber, J., Lim, D.A., Petritsch, C., Persson, A.I., Maunakea, A.K., Yu, M., Vandenberg, S. R., Ginzinger, D.G., James, C.D., Costello, J.F., Bergers, G., Weiss, W.A., Alvarez-Buylla, A., Hodgson, J.G., 2008. miR-124 and miR-137 inhibit proliferation of glioblastoma multiforme cells and induce differentiation of brain tumor stem cells. BMC Med. 6, 14–21.

Suli, A., Pujol, R., Cunningham, D.E., Hailey, D.W., Prendergast, A., Rubel, E.W., Raible, D.W., 2016. Innervation regulates synaptic ribbons in lateral line mechanosensory hair cells. J. Cell Sci. 129, 2250–2260.

Sun, L., Ling, Y., Jiang, J., Wang, D., Wang, J., Li, J., Wang, X., Wang, H., 2020. Differential mechanisms regarding triclosan vs. bisphenol A and fluorene-9-bisphenol induced zebrafish lipid-metabolism disorders by RNA-Seq. Chemosphere 251, 126318.

Szychowski, K.A., Sitarz, A.M., Wojtowicz, A.K., 2015. Triclosan induces Fas receptor-dependent apoptosis in mouse neocortical neurons in vitro. Neuroscience 284, 192–201.

Tian, X., Liu, Y., Wang, Z., Wu, S., 2021. miR-144 delivered by nasopharyngeal carcinoma-derived EVs stimulates angiogenesis through the FBXW7/HIF-1α/VEGF-A axis. Mol. Ther. Nucleic Acids 24, 1000–1011.

Wang, C., Huang, W., Lin, J., Fang, F., Wang, X., Wang, H., 2020. Triclosan-induced liver and brain injury in zebrafish (*Danio rerio*) via abnormal expression of miR-125 regulated by PKCα/Nrf2/p53 signaling pathways. Chemosphere 241, 125086.

Wang, H., Zhang, A., Wang, W., Zhang, M., Liu, H., Wang, X., 2013. Separation and determination of triclosan and bisphenol A in water, beverage, and urine samples by dispersive liquid-liquid microextraction combined with capillary zone electrophoresis-UV detection. J. AOAC Int. 96, 459–465.

Wang, T., Jin, J., Qian, C., Lou, J., Lin, J., Xu, A., Xia, K., Jin, L., Liu, B., Tao, H., Yang, Z., Yu, W., 2021. Estrogen/ER in anti-tumor immunity regulation to tumor cell and tumor microenvironment. Cancer Cell Int. 21, 123–131.

Wang, W., Peng, B., Wang, D., Ma, X., Jiang, D., Zhao, J., Yu, L., 2011. Human tumor microRNA signatures derived from large-scale oligonucleotide microarray datasets. Int. J. Cancer 129, 1624–1634.

Whitman, S.P., Maharry, K., Radmacher, M.D., Becker, H., Mrózek, K., Margeson, D., Holland, K.B., Wu, Y.Z., Schwind, S., Metzeler, K.H., Wen, J., Baer, M.R., Powell, B. L., Carter, T.H., Kolitz, J.E., Wetzler, M., Moore, J.O., Stone, R.M., Carroll, A.J., Larson, R.A., Caligiuri, M.A., Marcucci, G., Bloomfield, C.D., 2010. FLT3 internal tandem duplication associates with adverse outcome and gene- and microRNA-expression signatures in patients 60 years of age or older with primary cytogenetically normal acute myeloid leukemia: a cancer and leukemia group B study. Blood 116, 3622–3626.

Wienholds, E., Kloosterman, W.P., Miska, E., Alvarez-Saavedra, E., Berezikov, E., de Bruijn, E., Horvitz, H.R., Kauppinen, S., Plasterk, R.H.A., 2005. MicroRNA expression in zebrafish embryonic development. Science 309, 310–311.

Williams, J.A., 2019. Cholecystokinin (CCK) regulation of pancreatic acinar cells: physiological actions and signal transduction mechanisms. Compr. Physiol. 9, 535–564.

Witkowski, M., Pardyak, L., Pawlicki, P., Galuszka, A., Profaska-Szymik, M., Plachno, B. J., Kantor, S., Duliban, M., Kotula-Balak, M., 2021. The G-protein-coupled membrane estrogen receptor is present in horse cryptorchid testes and mediates downstream pathways. Int J. Mol. Sci. 22, 7131.

Xu, F., Wang, X., Wu, N., He, S., Yi, W., Xiang, S., Zhang, P., Xie, X., Ying, C., 2017. Bisphenol A induces proliferative effects on both breast cancer cells and vascular endothelial cells through a shared GPER-dependent pathway in hypoxia. Environ. Pollut. 231, 1609–1620.

Xu, J.J., Gao, P., Wu, Y., Yin, S.Q., Zhu, L., Xu, S.H., Tang, D., Cheung, C.W., Jiao, Y.F., Yu, W.F., Li, Y.H., Yang, L.Q., 2021. G protein-coupled estrogen receptor in the rostral ventromedial medulla contributes to the chronification of postoperative pain. CNS Neurosci. Ther. 27, 1313–1326.

Yueh, M.F., Tukey, R.H., 2016. Triclosan: a widespread environmental toxicant with many biological effects. Annu Rev. Pharm. Toxicol. 56, 251–272.

Zhang, L., Xiong, W., Fu, T., Long, X., Zhang, Z., Liu, Y., Lv, G., 2020. Oestrogen receptors and hypoxia inducible factor 1 alpha expression in abdominal wall endometriosis. Reprod. Biomed. 41, 11–18.

Zheng, Y., Wu, M., Gao, T., Meng, L., Ding, X., Meng, Y., Jiao, Y., Luo, P., He, Z., Sun, T., Zhang, G., Shi, X., Rong, W., 2020. GPER-deficient rats exhibit lower serum corticosterone level and increased anxiety-like behavior. Neural Plast. 5, 1–22.

Zhou, R., Yuan, P., Wang, Y., Hunsberger, J.G., Elkahloun, A., Wei, Y., Damschroder-Williams, P., Du, J., Chen, G., Manji, H.K., 2009. Evidence for selective microRNAs and their effectors as common long-term targets for the actions of mood stabilizers. Neuropsychopharmacology 34, 1395–1405.

Zhou, Y., Zhou, B., Pache, L., Chang, M., Khodabakhshi, A.H., Tanaseichuk, O., Benner, C., Chanda, S.K., 2019. Metascape provides a biologist-oriented resource for the analysis of systems-level datasets. Nat. Commun. 10, 1523–1532.

Zhu, J., Xia, R., Liu, Z., Shen, J., Gong, X., Hu, Y., Chen, H., Yu, Y., Gao, W., Wang, C., Wang, S.-L., 2020. Fenvalerate triggers Parkinson-like symptom during zebrafish development through initiation of autophagy and p38 MAPK/mTOR signaling pathway. Chemosphere 243, 125336.